



# Pollution transport and transformation over the Po Plain as revealed by airborne and ground-based measurements in July 2017 during EMeRGe

Costanza Civale<sup>1</sup>, M. Dolores Andrés Hernández<sup>1</sup>, Jean-Philippe Putaud<sup>2</sup>, Francesca Barnaba<sup>3</sup>, Henri Diémoz<sup>4</sup>, Johannes Schneider<sup>5</sup>, Helmut Ziereis<sup>6</sup>, Katharina Kaiser<sup>5,7</sup>, Jörg Schmidt<sup>8</sup>, Ovid Oktavian Krüger<sup>7</sup>, Bruna Holanda<sup>7</sup>, Robert Baumann<sup>6</sup>, Benjamin Weyland<sup>9</sup>, Eric Förster<sup>10,6</sup>, Midhun George<sup>1,x</sup>, Yangzhuoran Liu<sup>1</sup>, Daniel Sauer<sup>6</sup>, Jennifer Wolf<sup>6</sup>, Annachiara Bellini<sup>3,4</sup>, Birger Bohn<sup>11</sup>, Klaus Pfeilsticker<sup>9</sup>, and John Philip Burrows<sup>1</sup>

<sup>1</sup>Institute of Environmental Physics, University of Bremen, Bremen, Germany

<sup>10</sup>2European Commission, Joint Research Centre, Ispra, Italy

<sup>3</sup>National Research Council, Institute of Atmospheric Sciences and Climate (CNR-ISAC), Roma, Italy

<sup>4</sup>Regional Environmental Protection Agency (ARPA) of the Aosta Valley, Saint-Christophe, Italy

<sup>5</sup>Particle Chemistry Department, Max Planck Institute for Chemistry, Mainz, Germany

<sup>6</sup>Deutsches Zentrum für Luft- und Raumfahrt (DLR), Institut für Physik der Atmosphäre, Oberpfaffenhofen, Germany

<sup>15</sup>7Institute for Atmospheric Physics, Johannes Gutenberg University, Mainz, Germany

<sup>8</sup>Leipzig Institute for Meteorology, Leipzig University, Leipzig, Germany

<sup>9</sup>Institute for Environmental Physics, University of Heidelberg, Heidelberg, Germany

<sup>10</sup>Karlsruhe Institute of Technology, Institute of Meteorology and Climate Research, Karlsruhe, Germany

<sup>11</sup>Institute of Climate and Energy Systems, ICE-3, Forschungszentrum Jülich GmbH, 52428, Jülich, Germany

<sup>20</sup>x now at the School of Chemistry, University of Leeds, Leeds, LS2 9JT, UK

*Correspondence to:* M. Dolores Andrés Hernández (lola@iup.physik.uni-bremen.de)

**Abstract.** Airborne measurements provide valuable information about the vertical distribution of pollutants enabling the complex transport and dispersion pathways within and above the boundary layer (BL) to be investigated. In this study, the transport of pollution within the Po Plain, a major atmospheric pollution hotspot in Europe, was explored by exploiting airborne measurements made within the EMeRGe (Effect of Megacities on the transport and transformation of pollutants on the Regional to Global scales) project in combination with in situ and ground-based remote-sensing measurements over the whole Po basin. The analysis considers three areas where pollution emission and mixing are dominated by different processes: the Gulf of Venice to the east, the central part of the Po Plain, and the Gulf of Genoa to the west. Wind fields and backward trajectories during the days of the flights indicate the impact of the sea and mountain breezes on the BL distribution of pollutants, and of synoptic scale transport above it. Overall, the extensive data set of primary and secondary trace gases and aerosols at different altitudes provides insight into the effect of vertical and horizontal dynamical mixing on the chemical processing of pollutants within the BL. In this context, mixing of pollution plumes during stagnant conditions within the BL, stratification, venting and export of pollutants towards the Adriatic coast were observed. In addition, desert dust layers of Saharan origin at different altitudes confirm the mixing of naturally occurring dust and its impact on air quality of the lowermost atmosphere over the Po Plain.



## 1 Introduction

The Po Plain is the most densely populated area of Italy (Castaldini et al., 2019; Finardi et al., 2014) and its most important industrial and agricultural region. It comprises the administrative districts of Piedmont, Lombardy, Emilia-Romagna, Veneto, and Friuli Venezia Giulia, which comprise the urban agglomerations of Turin, Milan, Bologna, and Venice. With a population of approximately 20 million people (ISTAT, Annuario statistico Italiano 2022) and an average population density of 450 inhabitants  $\text{km}^{-2}$  (Castaldini et al., 2019; see also Sect. S1 in the supplement), the Po Plain is one of the European major population centres (MPC) (see <https://ineris.hal.science/ineris-00973562v1>; Molina and Molina, 2004; Gurjar and Lelieveld, 2005; Butler et al., 2012). The Po Plain is located in the north of Italy, and borders France, Switzerland, Austria, and Slovenia. It is bounded by the Alps to the north and west, by the Apennines to the south, which separates the plain from the Gulf of Genoa and the Ligurian Sea, and by the Gulf of Venice and the Adriatic Sea to the east (see Fig. 1). The topography of the area leads to a limited dispersion of air masses to the northern, western, and southern sides of the Po Plain, although regular pollution transport from the valley to the pre-alpine and alpine areas via a daily mountain-breeze circulation has been documented (Tampieri et al., 1980; Diémoz et al., 2019a, b). Overall, weak winds and intense solar radiation particularly in summer dominate the meteorological conditions in the Po Plain (e.g., Finardi and Pellegrini, 2004; Raffaelli et al., 2020). Frequent anticyclones cause subsidence of warm air in the mid-troposphere and the development of a stable temperature inversion that traps air pollutants in the boundary layer (BL) (e.g., Finardi and Pellegrini, 2004), leading to pollution episodes in both winter and summer months (Baklanov and Mahura, 2010; Finardi et al., 2014; EEA, 2019; Raffaelli et al., 2020). The high emission rates of pollutants from human activities e.g. industry, transport, domestic heating, use of air conditioning and agriculture (please note that the main emission sources are described in Sect. S2 of the supplement) combined with the topography of the area make the Po Plain one of the most polluted regions in Europe (e.g., Folberth et al., 2012; Gonzalez Ortiz et al., 2020, Targa et al., 2024).

Thermally- and pressure-driven circulation systems between mountains, plains, and the sea - such as mountain-valley circulation, sea breeze, and topographic venting from the BL to the free troposphere (FT) - cause complex patterns of the distribution of pollution (Henne et al., 2004). For example, pollutants emitted in the coastal areas (e.g., NO<sub>x</sub>, i.e., the sum of nitrogen monoxide NO and nitrogen dioxide NO<sub>2</sub>) are transported inland by sea-land breezes with pollutants emitted in the plain flowing towards the mountains, i.e., mountain venting (e.g. Diémoz et al., 2019a). Consequently, the oxidation of primary pollutants leads to the production of ozone (O<sub>3</sub>) and secondary aerosol along the mountain valleys (Henne et al., 2004; De Wekker et al., 2018). The compensating return circulation aloft subsides when flowing towards the sea, creating a vertical stratification in the upper coastal BL where O<sub>3</sub> and aerosols accumulate in the first 1-5 km altitude above the coast and offshore. Reservoirs of pollutants aloft are then subject to transport along the coast or form a pool in the mountain valleys and may partially be entrained into the surface level on the following day when the BL rises because of convection. This day-night circulation pattern usually has a turnover time of 2-3 days, similar to that found on the northeastern coast of Spain (Millán et al., 1997, 2000, 2002; Yus-Díez et al., 2021) and on the eastern and western coasts of Italy (Georgiadis et al.; 1994; Nyeki et

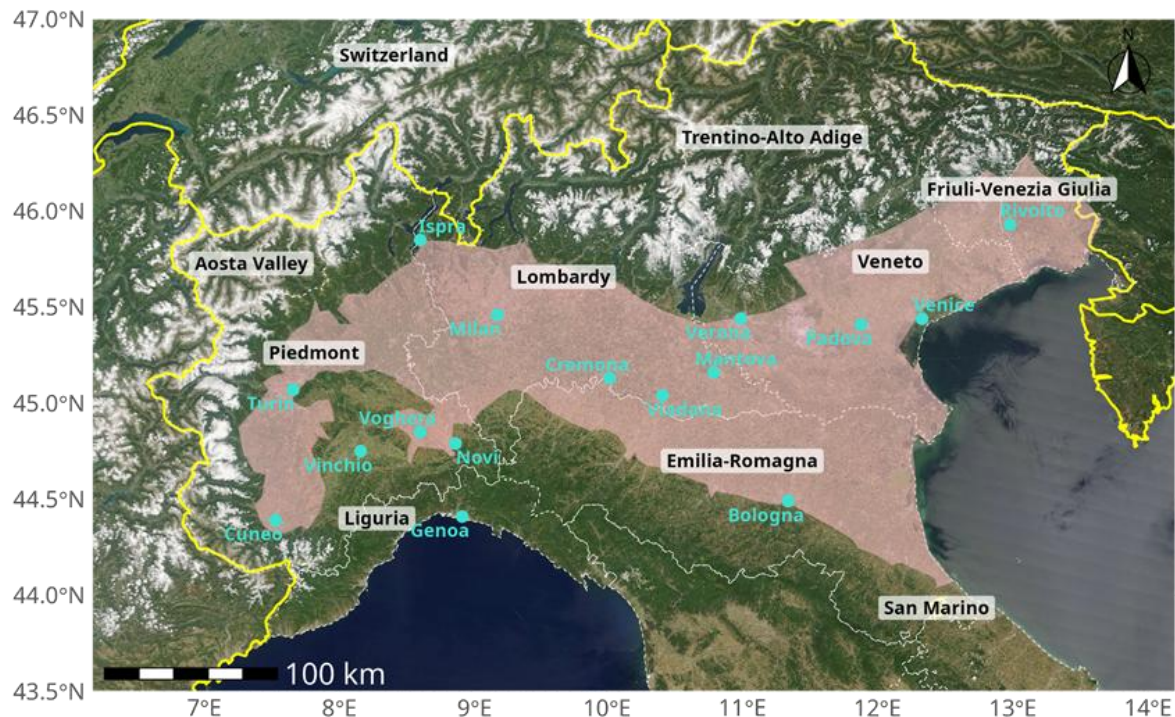


al., 2002; Finardi et al., 2018). A vertical export of air from the BL to the FT also occurs during venting events (Rotach et al., 70 2004). As a consequence, NO<sub>x</sub>-rich air mixes in the FT with the high background concentrations of methane (CH<sub>4</sub>) and carbon monoxide (CO) which is expected to increase the tropospheric O<sub>3</sub> column (Henne et al., 2004, 2005). The meso- or synoptic-scale horizontal mixing of air masses dominates the FT, contributing to the export of locally produced pollutants from the Po Plain to the north and east directions and above the Mediterranean basin. In this manner, the Po Plain pollution can affect the air quality of distant regions when re-entrained inside the BL (Henne et al., 2004; Weissmann et al., 2005; Diémoz et al., 75 2019a, b).

The atmospheric composition and distribution of pollutants in the Po Plain is constantly and extensively monitored at the surface and aloft by in-situ and remote-sensing observations (e.g., Folberth et al., 2012; Putaud et al., 2014; Ferrero et al. 2019; Gonzalez Ortiz et al., 2020, Bellini et al. 2024). Several studies targeting different pollutants and transport patterns from/to the Po Plain (e.g., Ambrosetti et al., 1998; Wotawa et al., 2000; Stortini et al., 2007; Highwood et al., 2007; Gohm et al., 2009; 80 Barnaba et al., 2007, 2010) have been published. The production and dispersion of pollutants from the Po Plain to the neighbouring regions have also been intensively investigated. Several projects and campaigns have shown the transport of pollution in the Italian Pre-Alps, Alps, the Adriatic Sea, and other Italian regions as well as transboundary transport into neighbouring countries (see Sect. S3 in the supplement).

However, the vertical distribution of pollutants within and above the BL is not sufficiently or adequately known, limiting our 85 knowledge of the complex transport and dispersion pathways in the Po Plain. The information provided by airborne measurements although snap shots and scarce is very valuable. In this context, airborne measurements in the Po Plain were carried out within the project EMeRGe (Effect of Megacities on the Transport and Transformation of Pollutants on the Regional to Global Scales) in July 2017 (Andrés Hernández et al., 2022). The objective of the EMeRGe measurement campaigns was to improve the current understanding of the photochemical and heterogeneous processing of pollution outflows 90 from MPCs by exploiting airborne measurements made on board the High Altitude and Long Range Research aircraft (HALO, <https://halo-research.de>).

The present study investigated the transport and transformation of pollutant emissions in the Po Plain by using aircraft borne and ground based instrumentation to extend our knowledge of summertime air pollution and the impact of the local dynamic. A key focus was to identify the dominant transport and transformation patterns in the targeted region and to assess the impact 95 of emissions from the diverse range of sources present. To achieve this goal, the EMeRGe airborne measurements of trace gases and aerosol particles in the lower troposphere and BL of the Po Plain were combined with those from relevant surface in situ and ground-based data from air quality measurement sites and research stations operating in July 2017 within the targeted area. Measurements of long-lived and reactive trace gases and particles were used to determine the time required for mixing and to assess boundary layer mixing dynamics.



100

**Figure 1: Northern Italy and relevant administrative regions (from west to east) of: Liguria, Piedmont, Lombardy, Emilia-Romagna, Veneto, and Friuli-Venezia Giulia. The Po Plain is highlighted in brown. The Alpine range surrounds the Po Plain on the north and west, and the Apennines in the southwest. Source: MODIS/Terra background from [worldview.earthdata.nasa.gov](http://worldview.earthdata.nasa.gov) (19 June 2017).**

The investigation explored three key topics:

105

- The horizontal distributions of selected pollutants in the BL over such a complex terrain and the effect of mixing on the vertical distribution of pollutants. One focus was the assessment of the information provided by airborne observations with respect to the BL composition and on the distribution of emissions at the ground.
- The identification of trans-regional and trans-boundary transport to and from the Po Plain.
- The performance of dispersion models using CO as a tracer to identify the origin and transport pathways of pollution in a complex topography.



## 2 Materials and methodology

### 2.1 Observational data

The present investigation exploited a set of airborne and ground-based observations obtained in July 2017 from instrumentation on different platforms having different temporal sampling and spatial resolutions.

#### 115 2.1.1 Airborne measurements of trace gases, aerosol particles, and meteorological variables

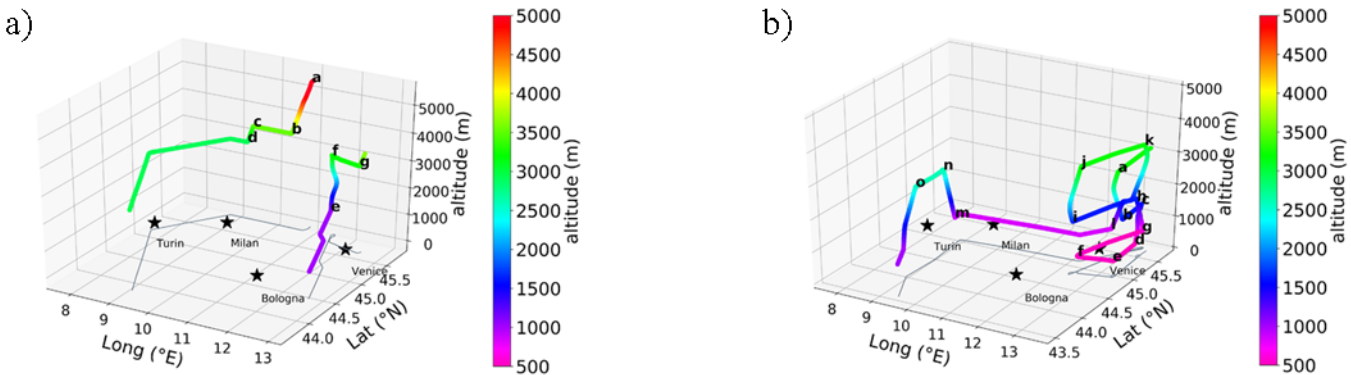
The HALO research aircraft was purchased as a result of a joint initiative of scientists at German universities and environmental and climate research institutions. It is owned and operated by the German Aerospace Centre (Deutsches Zentrum für Luft- und Raumfahrt/ Institute of Atmospheric Physics of the German Aerospace Center, DLR). HALO is a Gulfstream G550 business jet modified and specifically equipped for scientific research. During the EMeRGe campaign in Europe, the HALO aircraft 120 performed seven flights for a total of 53 flight hours covering a set of targeted MPCs in western Europe. A list of the in situ and remote-sensing instrumentation on board HALO used for the measurement of trace gases and aerosol particles as well as the basic aircraft data and ancillary measurements is provided elsewhere (Andrés Hernández et al., 2022). In the present study, only a subset of the trace gases measured by the HALO aircraft was selected to identify the transport of pollution in the BL. These were carbon monoxide (CO), carbon dioxide (CO<sub>2</sub>), sulphur dioxide (SO<sub>2</sub>), nitrogen monoxide (NO), total reactive 125 nitrogen (NO<sub>y</sub>), O<sub>3</sub>, acetone (C<sub>3</sub>H<sub>6</sub>O), and the total sum of hydroperoxy (HO<sub>2</sub>) and the organic peroxy (RO<sub>2</sub>) radicals which form NO<sub>2</sub> in their reaction with NO (defined as RO<sub>2</sub><sup>\*</sup>). Non-refractory nitrate (NO<sub>3</sub><sup>-</sup>), sulphate (SO<sub>4</sub><sup>2-</sup>), ammonium (NH<sub>4</sub><sup>+</sup>), total organic aerosol (OA), m/z 44 as a marker for oxidized organic aerosol (OOAm), and refractory black carbon (rBC) in the submicron aerosol fraction, as well as the particle number size distribution (from 10 nm to 2.5  $\mu$ m) were additionally measured in situ. Nitrogen dioxide (NO<sub>2</sub>) and formaldehyde (HCHO) were measured using an airborne mini-DOAS (Differential Optical 130 Absorption Spectrometer) with a temporal sampling of 1 min. For clear skies the averaging volume of the NO<sub>2</sub> miniDOAS measurements is estimated in the vertical direction by the field of view of the telescope and in the horizontal view by the distance the aircraft travelled during integration (~7 km), while both are modulated by the average light path length perpendicular to the aircraft direction of flight. The latter ranges between 10 km to 25 km near the ground with considerably shorter photon path lengths occurring in the aerosol loaded and cloudy atmosphere. This inherent radiative transfer related 135 averaging may smooth the actual mixing ratios over the observing kernel depending on the location of the pollutant layers with respect to the aircraft (for details, see Hünemeier et al., 2017 and Kluge et al., 2020).

Two EMeRGe flights, E-EU-03 and E-EU-06, were carried out over the same geographical region and targeted specifically the Po Plain on 11 and 20 July 2017, respectively. Initially, HALO flew over the Alps, then along the Po Valley to the Mediterranean coast of Italy crossing the Italian Peninsula from west to east over Rome and then north to the Alps along the 140 Adriatic coast back to the HALO base in Germany (Andrés Hernández et al., 2022). Only the flight tracks that overflow the Po Plain were considered in this study, and are shown in Fig. 2. Letters and numbers are used to indicate the waypoints of the flight tracks (i.e. 6a to 6o for E-EU-06, see Supplement Sect. 4 and Table S4 therein for full details). The vertical and horizontal



distribution of pollutants were investigated by flying at lower altitudes and incorporating shuttles (i.e., descent or ascent flight patterns between holding altitudes) in the tracks.

145



150 **Figure 2: Flight tracks from the EMeRGe flights a) E-EU-03 on 11 July 2017, and b) E-EU-06 on 20 July. The colour-code refers to flight altitude during the flight tracks considered in this study and the letters indicate the waypoints as mentioned in the text. All altitudes are above sea level (asl). The 2D flight track is shown in grey on the xy plane, main cities in the area are also reported (black stars) to facilitate geo-reference and comparison with Fig.1.**

### 2.1.2 In-situ surface and ground-based remote sensing measurements

In Italy, air quality is monitored at the regional level by the local Environmental Protection Regional Agencies (ARPA) 155 measuring EU-legislated pollutants and meteorological variables in air quality networks (see Sect. S5 and S6 in the supplement). In this work, the hourly resolved data from ARPA traffic and background air quality monitoring network (AQMN) stations located in the proximity to the HALO flight tracks in the regions of Piedmont, Lombardy, Veneto, and Liguria were used (see Fig. 3). In addition, trace gas measurements of high accuracy and 10-minute temporal sampling were provided by the regional background atmospheric observatory of the European Commission's Joint Research Centre (EC-JRC) in Ispra (<https://abc-is.jrc.ec.europa.eu/>).

Aerosol profiles from selected ground-based active remote-sensing stations were used in support of the analysis (see S7 in the 160 supplement). These were obtained by an aerosol LiDAR (Light Detection and Ranging) operating in Ispra in association with ACTRIS (Aerosol, Clouds and Trace gases Research Infrastructure, [www.actris.eu](http://www.actris.eu)), and by an automated LiDAR-ceilometer (ALC) operating in Milan as part of ALICENET (Italian Automated LiDAR-CEliometer NETwork, [www.alice-net.eu](http://www.alice-net.eu), Bellini et al., 2024). Both LiDAR and ALC profiles of the particle backscatter coefficient ( $\beta_p$ ) provided information about the presence 165 of different aerosol stratifications within the BL and in the FT (see Fig. 3 for instrument location). In Ispra, profiles of the particle depolarisation ratio ( $\delta_p$ ) at specific measurement times were used to identify the presence of desert dust (particles of non-spherical shapes) within some specific aerosol layers (Wandinger, 2005), while high temporal sampling and continuous ALC profiles enabled the diurnal variability of the aerosol structures to be identified and the relevant diurnal evolution of the



Mixed Aerosol Layer (MAL) to be inferred (in cloud-free conditions only) following the approach described in Bellini et al., (2024).

170 **2.1.3 Meteorological soundings**

The radiosonde stations selected for this study were Cuneo Levaldigi, Milano Linate, and Rivolto (see Fig. 3). For the determination of the height of the BL, two different methods were applied to the radiosonde in situ measurements of temperature (T), potential temperature ( $\Theta$ ) and relative humidity (RH) at 12 UTC on the days of flight. In the parcel method, the BL height is either defined as the elevation at which an ascending air parcel becomes neutrally buoyant (Hennemuth and 175 Lammert, 2006) or to which an air parcel with surface temperature rises adiabatically from the ground by convection (Collaud Coen et al., 2014). The height of the BL is calculated as the intersection between the temperature profile and the dry adiabatic lapse rate starting at near-surface temperature (Seibert et al., 2000; Collaud Coen et al., 2014). In contrast, the gradient method defines the BL height as the height where the gradient of  $\Theta$  is maximum (T gradient method), corresponding to the top of the capping inversion, or where the gradient of the RH is minimum or zero (RH gradient method), associated with a reduction in 180 water vapour content (Hennemuth and Lammert, 2006; Wang and Wang, 2014). Among the methods applied to the radiosonde profiles to estimate the BL, the parcel method is considered the most reliable, but it has proven to fail when applied to a stable BL over land or sea. A cloud-topped BL is also hardly identifiable because of the complex structure associated with cloud layers (Seibert et al., 2000; Hennemuth and Lammert, 2006). Despite the limitations of single radiosonde profiles to describe the changes in space and time of the vertical structure of the atmosphere and to identify the limits of the BL in the presence of 185 cloud layers (e.g., Seibert et al., 2000; Hennemuth and Lammert, 2006), both methods agreed reasonably well for measurements made on the days studied.

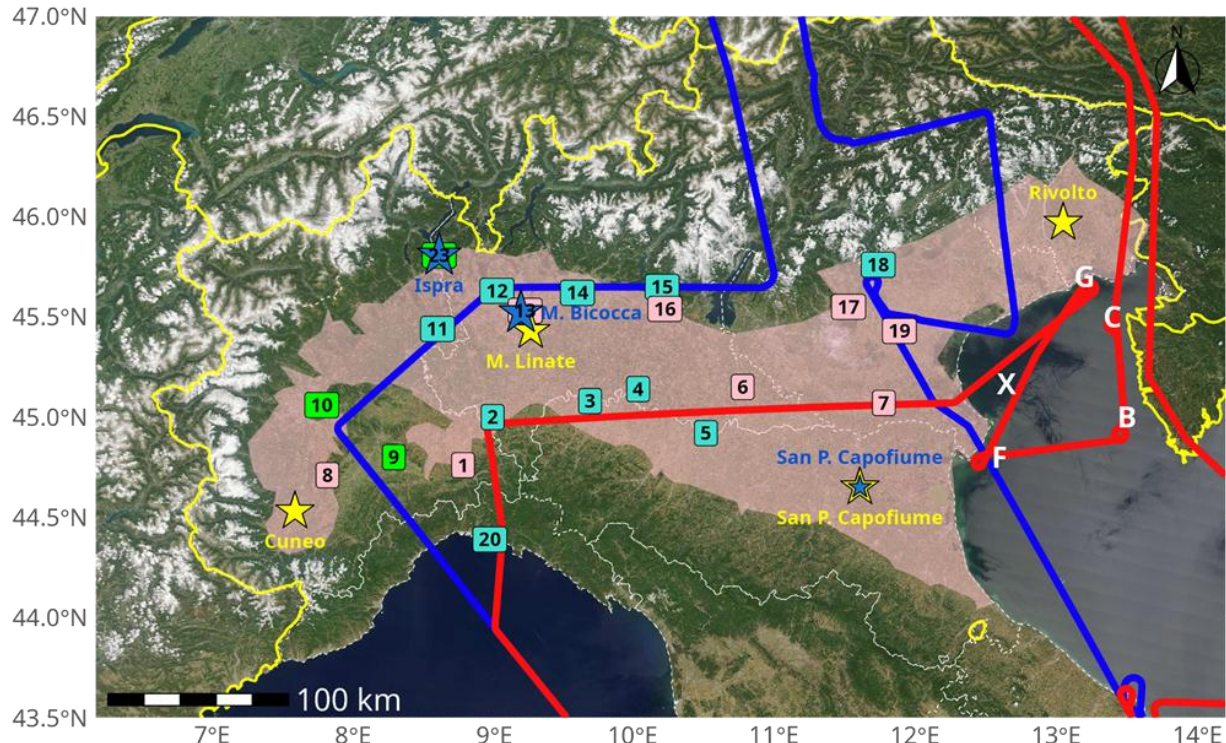


Figure 3: Data sources used in this study, covering the whole area of the Po Plain: E-EU-03 (blue) and E-EU-06 (red) HALO flight tracks; AQMN traffic (pink squares), urban background (turquoise squares) and regional background (green squares) stations are identified by the station number; radiosonde stations (yellow star) and LiDAR/ALC stations (blue star). Geographical points indicated by white capital letters are used in the discussion of the E-EU-06 track (see Sect.3).

## 2.2 Modelled estimation of transport patterns of pollution

The data interpretation and the estimation of pollution transport patterns during the E-EU-03 and E-EU-06 flights rely on the prevailing meteorological conditions before and during the measurements to determine the origin of the air masses probed. Following model-based tools were used:

a) FLEXTRA: backward trajectories

The FLEXTRA backward-trajectories provided for EMeRGe were calculated with the FLEXTRA 5.0 trajectory model (see Stohl et al., 1995; Stohl and Wotawa, 1995; <https://folk.nilu.no/~andreas/flextra.html>), using the European Centre for Medium-Range Weather Forecast (ECMWF, <https://www.ecmwf.int/>) operational data set ERA5 meteorological data (see Hersbach et al., 2020) at 0.25° horizontal resolution (around 27.8 km). Trajectories were initialised every minute of the flight time and cover the trajectory over the 10 days prior to the locations.

b) COSMO: wind fields

The COSMO-Model (Consortium for Small-scale Modeling, <http://www.cosmo-model.org>) which uses a 10 times finer step grid than that of ERA5, was additionally employed in this study to ensure an accurate analysis of transport dynamics on the



mesoscale, such as the valley-mountain breeze. COSMO is a non-hydrostatic, fully compressible, limited-area atmospheric prediction model. It is based on thermo-hydrodynamical equations for compressible flow in a moist atmosphere, formulated in rotated geographical coordinates and a generalized terrain following height coordinates. The data used by COSMO were provided for the period under investigation by the meteorological operational centre – air force meteorological service 210 COMET. The present study considers the high-resolution version COSMO-I2 or COSMO-IT (2.8 km grid cells and 65 vertical levels) in its numerical weather prediction declination for the assessment of the wind field in the Po Plain area. Notably, as complete 3D fields (surface and vertical profiles) are released at 6-hour intervals, the wind fields simulated at 09 and 12 UTC on 11 and 20 July were used, with altitude steps of 200 m between ground level and 2000 m. The origin of air masses is 215 assessed in combination with the Lagrangian tool LAGRANTO (Sprenger and Wernli, 2015) integrating the COSMO wind fields and tracing 3-D backward-trajectories for air masses. For this study, 12 hours backward-trajectories were computed with a time step of 15 minutes, starting from the aircraft coordinates.

c) HYSPLIT: CO enhancements during transport

The Lagrangian Particle Dispersion Model HYSPLIT (Marenco et al., 2006; Birmili et al., 2010; <https://www.arl.noaa.gov/hysplit/>) calculates the atmospheric dispersion of local emissions of CO, accumulated over 6 days 220 of transport. HYSPLIT simulations were used to estimate the contribution of CO emissions within the Po Plain (44-46N, 7.5-13.5E) at the time and place of the CO measurements aboard HALO, as well as the ages of the emissions. The HYSPLIT simulated CO concentrations do not include accumulated "background" values due to the much longer lifetime of CO and are therefore not to be compared with absolute concentrations but rather with CO enhancements (i.e.,  $\Delta$ CO) in local plumes. HYSPLIT was driven by meteorological data from the operational ECMWF forecast (0-11 hours forecast, 12-hourly update, 225 interpolated at 0.1° horizontally, pressure levels, 1-hourly output). CO emission rates were taken from the EDGAR HTAP V2 emission inventory ([http://edgar.jrc.ec.europa.eu/htap\\_v2/](http://edgar.jrc.ec.europa.eu/htap_v2/)). Neither chemical reactions nor convection are modelled. The computation (core-model) and the visualisation (post-processing) were controlled by a specific client-server infrastructure developed at the Institute of Atmospheric Physics of the DLR for campaign support as well as post-campaign analysis.

### 3 Results and discussion

230 A main focus of the analysis is on the distribution of pollutants within the BL of the Po Plain. For this, the BL height was calculated from the air parcel and gradient methods applied to the radiosonde measurements in each station (see Table 1). Due to the presence of clouds, the RH gradient method underestimated the BL depth on 20 July and was thus not used for the BL estimate. The BL height values obtained in Table 1 are consistent with the available ground-based aerosol profile measurements.

235 According to the weather reports provided by the corresponding ARPAs, the weather was unstable on 11 July because of the passage of a low-pressure system, which came from Great Britain in the NW. The on-board measured photolysis frequency  $j_{NO_2}$  was used as a qualitative surrogate for cloudiness during the flights while the vertical wind speed (vws) measured by



240 **Table 1: Average BL height at 12:00 UTC as estimated by using the parcel, the temperature gradient, and the relative humidity methods to the radiosonde measurements in Milano Linate, Cuneo Levaldigi, and Rivolti on the 11 and 20 of July. On 11 July the values are derived from the average of the three methods described in the Sect. 2.1 while the parcel and temperature gradient methods are used for the 20 July. The uncertainty on the values is the maximum error ((max value – min value)/2).**

	11 July 2017	20 July 2017
<b>Milano Linate</b>	$1450 \pm 100$ m	$1600 \pm 400$ m
<b>Cuneo Levaldigi</b>	$1340 \pm 80$ m	No measurement available
<b>Rivolti</b>	$1710 \pm 180$ m	$1000 \pm 70$ m

245 HALO at the flight altitude was taken as an indicator of vertical mixing within the BL (Fig.4). As expected, the measured  $j_{NO_2}$  was lower when the E-EU-03 flight approached regions of unstable weather and turbulence in the surroundings of Cuneo (11-11:50 UTC) and Padova (from 15:15 UTC onward). This instability may have favoured the vertical dilution of emitted pollution in comparison to the 20 July, when the presence of a desert dust layer may have concurred in stabilizing the atmosphere. During the E-EU-06, a pronounced  $j_{NO_2}$  variability was observed during passage through a cloud-covered sky south of Milan (around 12 UTC). The vertical wind speed was low ( $< 0.5$  m s $^{-1}$ ) as was its variability above the sea over the Gulf of Genoa, and ranged from -2 to +4 m s $^{-1}$  (1 s values) over land in the central Po Plain at 830-840 m approximately.

250

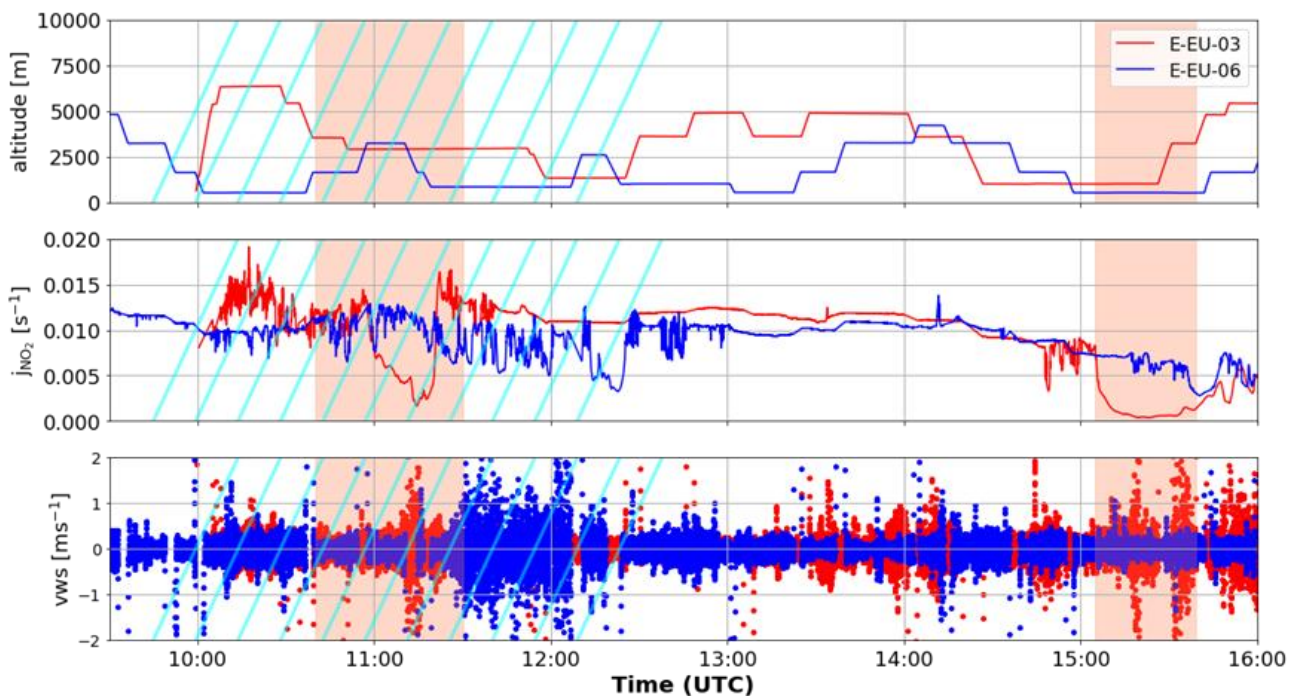


**Figure 4: Photolysis frequency ( $j_{NO_2}$ ), flight altitude and vertical wind speed (vws) measured during the E-EU-03 flights (red) and the E-EU-06 flight (blue). The periods of the two flights above the Po Plain are shaded in coral and striped in cyan, respectively.**



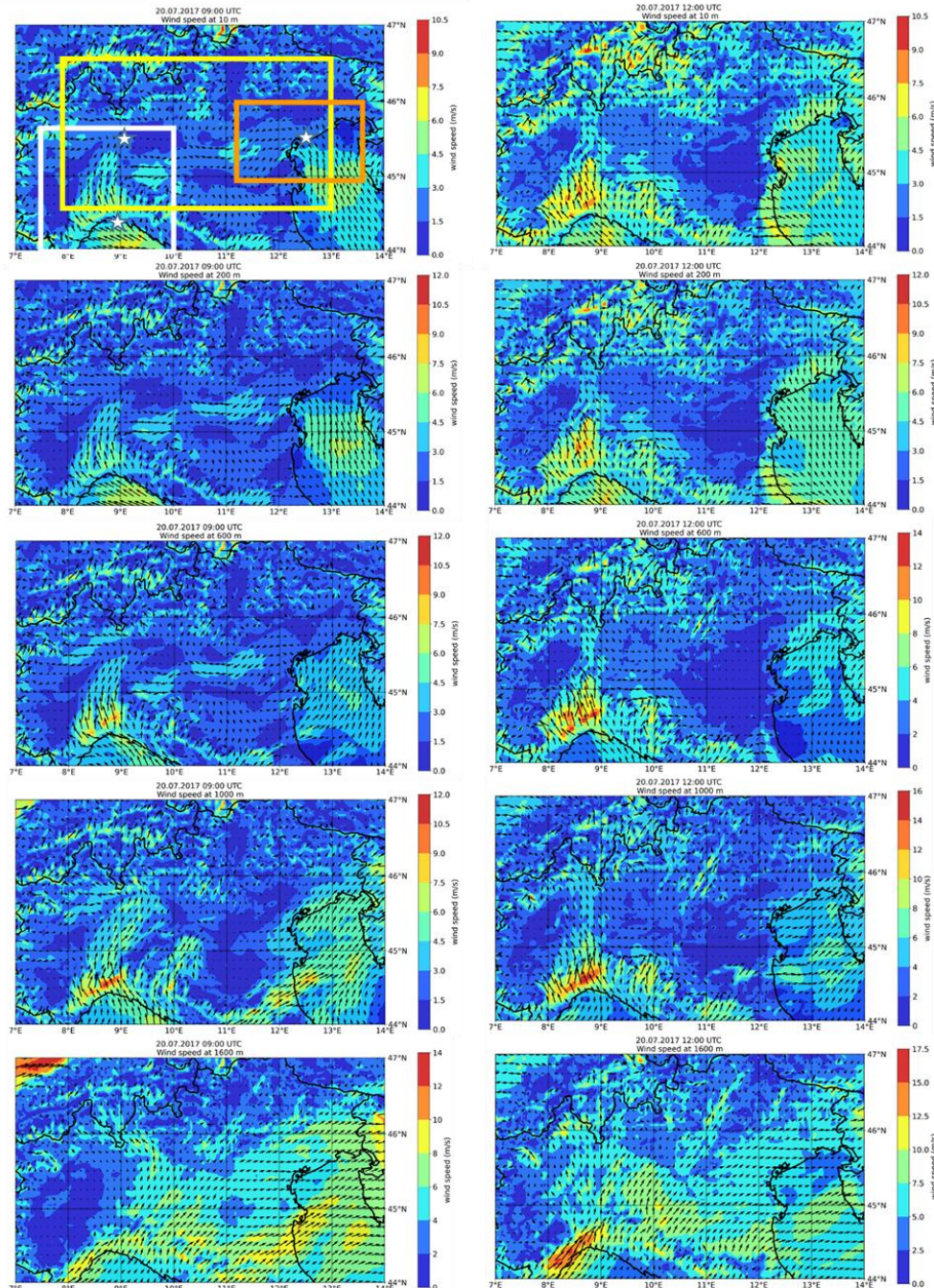
In Fig. 5, the wind circulation calculated by COSMO for the 20 July E-EU-06 EMeRGe flight at 9 and 12 UTC provides evidence for the complex thermally and orographically driven air transport patterns over the Po Plain (see Sect. S9 in the supplement for the 11 July E-EU-03 flight). Inside the BL, sea breeze regimes are observed, with stronger winds increasing with altitude at the west coast (43.5–45° N; 8–10° E) and sea to land circulation up to approximately 600 m altitude at the east coast (44–46° N; 12–14° E). In the upper layers of the BL (ca 800–1000 m), an inland-bound breeze flows from the west coast to the mountains (8–10° E, 46° N) at 9:00 UTC and is still visible with slight changes in intensity and wind direction at 12 UTC. In the FT, the model computed eastwards to north-eastwards air transport, following the dominant pattern observed over the Po Plain (Finardi et al., 2004 and Diémoz et al., 2019a, b), revealing a strong wind shear between ~1000 and 1600 m asl. As HALO remained during the E-EU-03 above the BL except for the last flight tracks late in the afternoon, further data analysis will focus on E-EU-06. The investigated region was divided into three geographical partly overlapping areas (see Fig. 5 top left) marked by different mixing regimes: the two coastal areas of the Gulf of Venice (44.5–46° N; 11.5–13.5° E) and the Gulf of Genoa (43.5–45.5° N; 7.5–10° E), and the central part of the Po Plain (44.5–46.5° N; 8–13° E). These areas of study will hereafter be referred to as GV, GG, and CPP, respectively.

### 3.1 Pollutant distribution and gradients within the BL during E-EU-06 on 20 July 2017

The airborne trace gas and aerosol particle concentrations were analysed in the three selected areas of the Po Plain during the E-EU-06 flight to assess vertical gradients and the degree of mixing in the BL between 9:45 and 12:30 UTC. Information about the vertical distribution of pollutants at the time of the flight was provided by measurements at different altitudes during the HALO shuttles.

Increases in the airborne mixing ratios of NO<sub>y</sub>, O<sub>3</sub>, and CO as well as in rBC and particulate nitrate concentrations inside the BL were attributed to HALO flying through plumes of pollution. Short-term variations in the relative concentrations of trace gases provided additional information about the origin and chemical transformation of the plumes during transport. In particular, the HCHO to NO<sub>2</sub> ratio is an indicator of the sensitivity of O<sub>3</sub> photochemical formation to NO<sub>x</sub> and VOC concentrations in the atmosphere. HCHO is an intermediate formed in the oxidation of most VOC and is often used as a proxy for the total VOC reactivity (Sillman, 1995). The HO<sub>2</sub> formed by HCHO photolysis increases the rate of catalytic cycling of NO to NO<sub>2</sub>. A HCHO / NO<sub>2</sub> < 1 indicates a VOC-limited regime while a HCHO/NO<sub>2</sub> > 4 indicates a NO<sub>x</sub>-limited regime (e.g., Souri et al., 2020; Hong et al., 2023, Vazquez Santiago et al., 2024).

The effective mixing of freshly emitted and aged pollution was evaluated from HYSPLIT CO dispersion simulations. The CO enhancement provided by HYSPLIT ( $\Delta$ CO) is used as an indicator of the contribution of the CO emissions within the Po Valley as well as of the age of the air masses mixed before the CO measurement point.



285 **Figure 5:** Wind speed and direction from 10 m (top) to 1600 m (bottom) altitude above ground level (agl) simulated by COSMO on 20 July 2017 at 9:00 UTC (left) and 12:00 UTC (right) in Northern Italy. Boxes in the top left panel indicate the three geographical areas selected for this study: the Gulf of Venice (GV, red), the Gulf of Genoa (GG, white) and the central Po Plain (CPP, yellow). Sea-land circulation dominates on the ground in the coastal areas and reverses in the GV from about 600 m. Please note the changes in the scale of the wind speed (ws). White stars indicate the position of Genoa, Milan and Venice (from left to right).



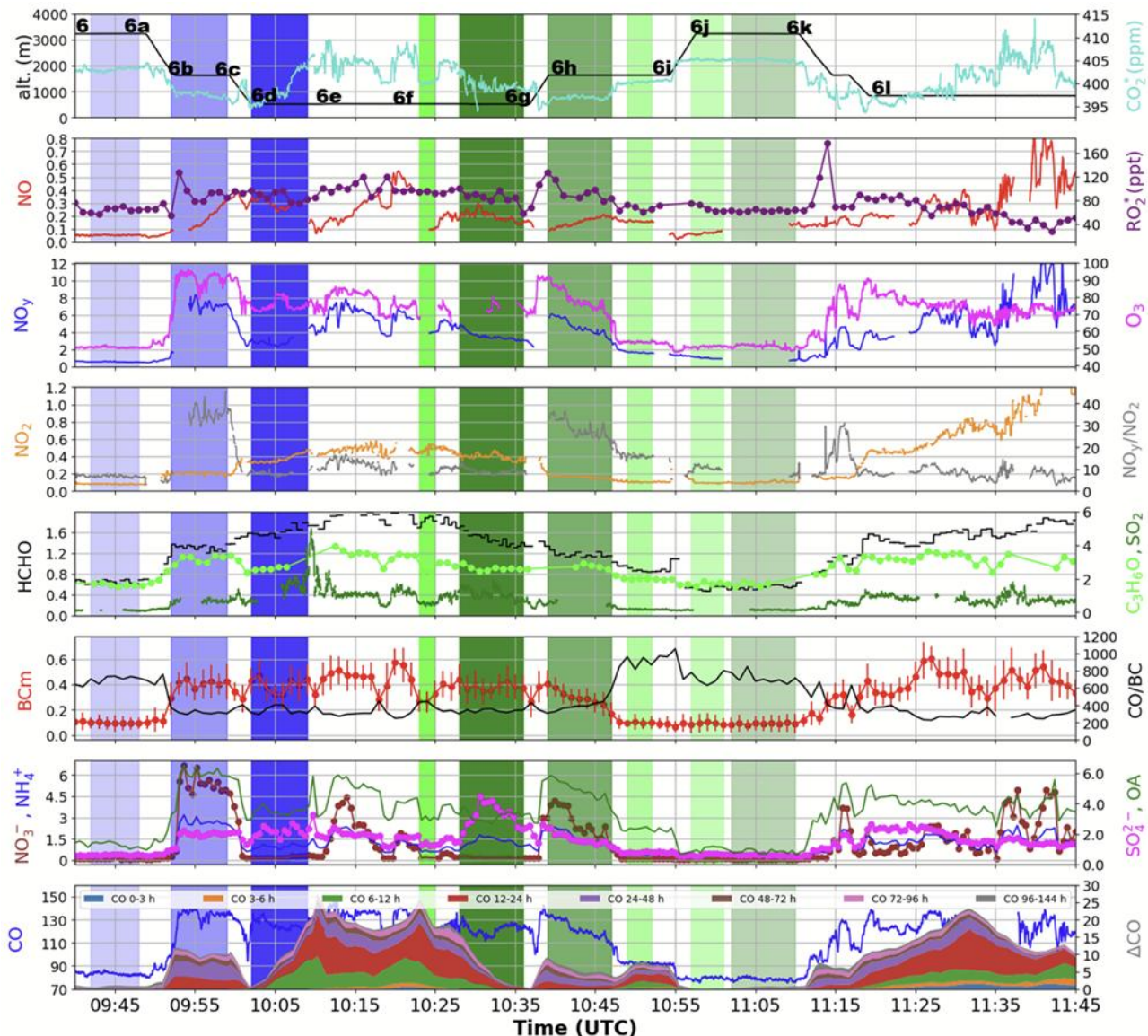
290 **3.1.1 Vertical distribution and advection of pollutants in the Gulf of Venice (GV)**

Figure 6 shows the temporal variation of NO, NO<sub>y</sub>, NO<sub>2</sub>, O<sub>3</sub>, CO, HCHO, C<sub>3</sub>H<sub>6</sub>O, SO<sub>2</sub>, RO<sub>2</sub><sup>\*</sup>, CO<sub>2</sub> mixing ratios, and rBC, OA, NO<sub>3</sub><sup>-</sup>, NH<sub>4</sub><sup>+</sup>, and SO<sub>4</sub><sup>2-</sup> mass concentrations measured on board HALO over the GV during the EMeRGe E-EU-06 flight. Measurements made over the same GV area at different heights are shaded with the same colour (darker shades at lower altitudes). Between 09:40 and 11:35 UTC HALO remained within the BL below 600 m between the waypoints 6d and 6g and 295 below 850 m after waypoint 6l (Fig. 6). Two shuttles were carried out over the GV:

- 1) from 09:42 to 10:10 UTC between **B** (45.0°N, 13.4°E) and **C** (45.4°N, 13.5°E) about 100 km off the Italian coast and along the Croatian west coast (see Fig. 3) at 3230 m asl (6 to 6a), 1630 m (6b to 6c) and 520 m (6d to 6e),
- 2) from 10:21 to 11:19 UTC between **F** (44.9°N, 12.6°E) and **G** (45.6°N, 13.1°E) less than 35 km off the Italian coast at 520 m (6f to 6g), 1630 m (6h to 6i), and 3230 m (6j to 6k).

300 In Fig. 7, the 3D distributions of CO, SO<sub>2</sub>, O<sub>3</sub> and NO are plotted for shuttles 1 (waypoints 6 to 6e) and 2 (waypoints 6f to 6j). The transect between both shuttles in the marine BL across the Adriatic (6e to 6f) is analysed separately in 3).

- 1) During the first shuttle (between points **B-C** in Fig. 3), the concentrations of gaseous and particulate species were deemed constant enough during the slots selected for each of the legs 6-6a, 6b-6c and 6d-6e to be averaged. The values measured for several species including CO, O<sub>3</sub>, C<sub>3</sub>H<sub>6</sub>O, particulate OA, NO<sub>y</sub> and particulate NO<sub>3</sub><sup>-</sup> are higher at 1630 m asl in 305 the FT (6b-6c) than at 530 m asl (6d-6e) in the BL. This is not the case for NO, NO<sub>2</sub>, SO<sub>2</sub>, HCHO, particulate SO<sub>4</sub><sup>2-</sup> and rBC (Fig. 6). As a consequence, NO<sub>y</sub>/NO<sub>2</sub> ratios were high at 1630 m levels (6b-6c). At 3230 m asl, mixing ratios are less than in the BL for all species. Backward trajectories and wind maps suggest advection of FT air masses (> 2000 m) at 3230 m and of marine BL air masses at 520 m, as well as lifting of BL air masses originating from CPP at 1630 m. Larger O<sub>3</sub>/CO, C<sub>3</sub>H<sub>6</sub>O/CO, NO<sub>y</sub>/CO, NO<sub>y</sub>/NO<sub>2</sub>, particulate NO<sub>3</sub><sup>-</sup>/rBC and OOAm/rBC ratios (see Fig. 8 and Table S8 in the supplement) indicate increased 310 concentrations of secondary pollutants, characteristic of photochemically processed air masses across this leg. Furthermore, the HYSPLIT calculation of the CO enhancement also implies a significant contribution (10 ppbv) of emissions from the Po Valley primarily from the previous 12-48 hours for this leg (Fig. 6). HCHO/NO<sub>2</sub> ratios (not shown) increased from 4 at 520 m, to 6 at 1630 m, and 8 at 3230 m, indicating that O<sub>3</sub> photochemical production becomes increasingly NO<sub>x</sub> limited with altitude during this shuttle along the Croatian coast. The highest SO<sub>2</sub> mixing ratios were observed when approaching waypoint 315 6e (530 m asl) close to the Croatian coast at ~10:10 UTC. These could be explained by a contribution from shipping (cargo ships and cruise ferry traffic) as the main sources of gaseous pollutants in the GV (see <https://www.port.venice.it/en/projects-and-sustainability/>). The NO and NO<sub>y</sub> data are not available at this time due to instrumental zero calibration. Backward trajectories indicate that air masses were lifted up from the sea surface to 520 m, 10-16 hours before the measurements.



320

**Figure 6:** Temporal variation of NO, NO<sub>y</sub>, NO<sub>2</sub>, O<sub>3</sub>, CO, HCHO, C<sub>3</sub>H<sub>6</sub>O, SO<sub>2</sub> (all in ppbv, units not written in the axis for clarity), RO<sub>2</sub><sup>\*</sup> (in pptv), CO<sub>2</sub> (in ppm) mixing ratios, and rBC, NO<sub>3</sub><sup>-</sup>, NH<sub>4</sub><sup>+</sup>, SO<sub>4</sub><sup>2-</sup> and OA mass concentrations (in  $\mu\text{g m}^{-3}$  STP) measured on board HALO over the Gulf of Venice (GV) during the EMERGE E-EU-06 flight. HCHO and NO<sub>2</sub> values are retrieved from miniDOAS measurements. BCm are 1 min averages of rBC with  $1\sigma$  error bars. The flight altitude and the changes in course and altitude (waypoints 6-6l) are marked in the top panel. Blue, lime and green shaded coloured time windows highlight air masses each captured over the same geographical area (see Figure 13) but at different heights (darker at lower altitudes). HYSPLIT simulations of the contribution of Po Valley emissions to the observed ( $\Delta\text{CO}$ ) coloured according to the estimated age are shown in the bottom panel.

325

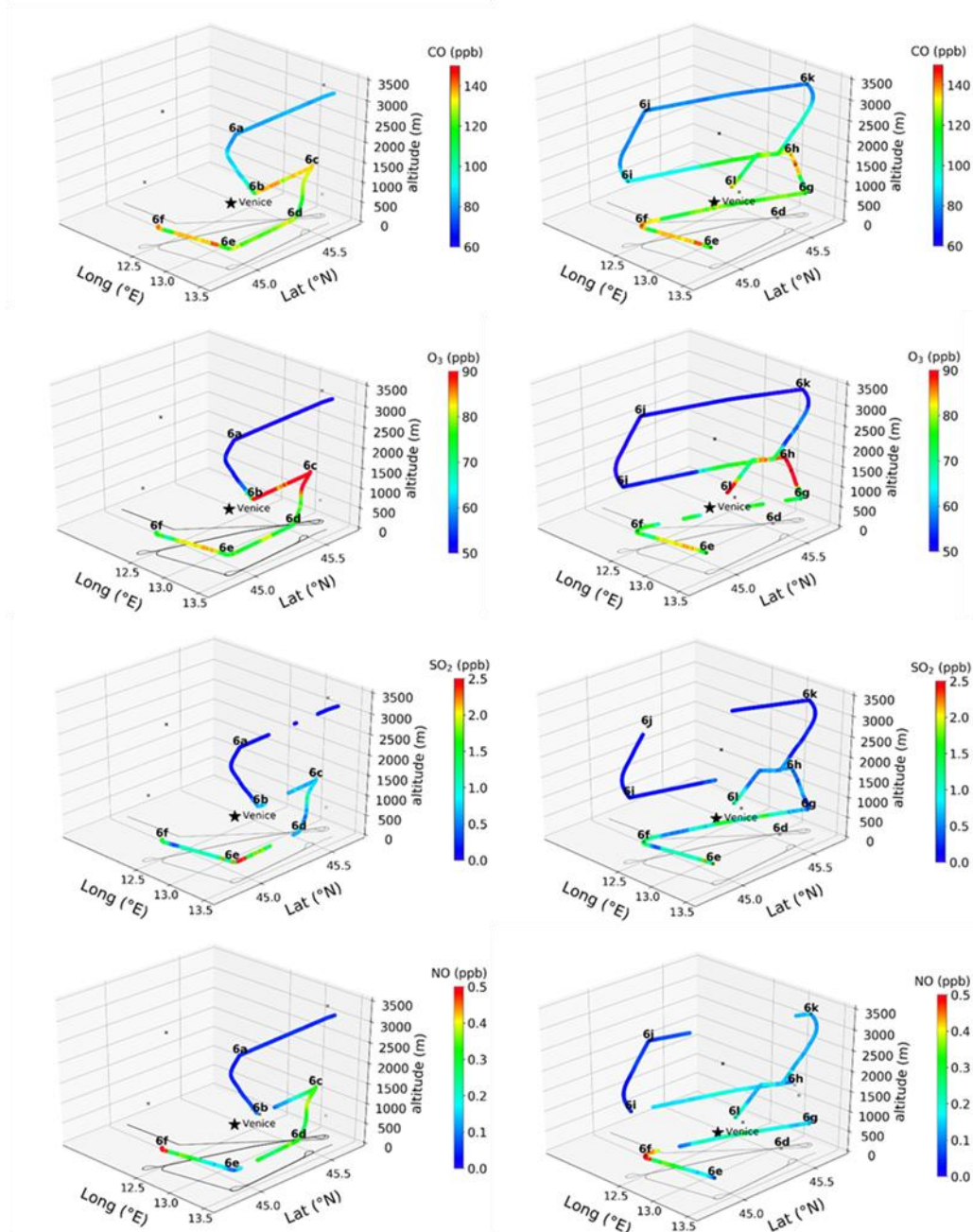
2) During the second shuttle across GV, near the Italian coast (between points F-G in Fig. 3), the concentrations of the 330 gaseous and particulate species changed significantly between waypoints 6h and 6i at 1630 m asl. Each leg of the shuttle is covering the same spatial area but in the opposite temporal order, so that the area at the end of the leg at 520 m is overflowed



at the beginning of the leg at 1630 m and again at the end of the leg at 3230 m (see also HALO tracks in Fig. 2b). As indicated above, observations over the same GV area at different heights are shaded with the same colour (darker shade at lower altitudes) in Fig. 6. Further analysis was undertaken by splitting in two the legs between **F** and **G** at point **X** (Fig. 3),  
335 thus north and south of 45.13°N.

Similarly to the first shuttle, significant enrichments in the FT at 1630 m asl compared to those in the BL (520 m) were observed north of point X in the oxidised nitrogen species ( $\text{NO}_y$ ,  $\text{NO}_3^-$ ), and total OA. Mixing ratios/mass concentrations at these two altitudes were similar for CO, NO,  $\text{O}_3$ ,  $\text{C}_3\text{H}_6\text{O}$ , and rBC, whereas they were significantly lower at 1630 m for  $\text{NO}_2$ , HCHO,  $\text{SO}_2$ , and  $\text{SO}_4^{2-}$  (Fig. 8). At 3230 m the concentrations or mixing ratios of all species were lower. Particularly high  $\text{NO}_y/\text{CO}$ ,  
340  $\text{NO}_y/\text{NO}_2$ ,  $\text{NO}_3^-/\text{rBC}$ , OA/rBC and OOAm/rBC ratios north of point **X** at 1630 m asl indicated a highly processed pollution plume. Backward trajectories ending at this leg of the aircraft track crossed the Po Valley at about 1500 m agl during the previous 6 hours, and passed at ~1000 m agl in a region around 44.5° N, 10.0° E about 12 hours before the measurements. This is consistent with the HYSPLIT simulations that indicate a predominant contribution of emissions older than 24 h to a  
345 moderate (5 ppb) CO enhancement. In contrast with carbon and nitrogen compounds, sulphur compounds ( $\text{SO}_2$  and  $\text{SO}_4^{2-}$ ) were not enhanced in the plumes probed at 1630 m asl. In particular,  $\text{SO}_2$  mixing ratios and  $\text{SO}_2/\text{CO}$  were a factor of ~2 lower at 1630 m compared to 520 m asl, which is consistent with sulphur-poor emissions and/or sulphur sinks such as oxidation by OH or uptake by dust or cloud droplets inside the BL. CO is expected to have a significantly longer lifetime than  $\text{SO}_2$  because it is less water-soluble and the rate of removal of CO by the reaction with OH is much lower than that for  $\text{SO}_2$ . However, the lack of enhancement in  $\text{SO}_4^{2-}$  suggests that  $\text{SO}_2$  oxidation followed by gas-to-particle conversion did not play a major role.

350 Particularly high  $\text{SO}_2$  mixing ratios and  $\text{SO}_2/\text{CO}$  ratios were observed in the BL (520 m asl) during this leg. Backward trajectories indicate that air masses travelled in the BL below 520 m asl during the previous 24 hours, pointing at shipping as a major source of  $\text{SO}_2$ . Port traffic and activities around the port of Venice have been found to impact negatively on the local air quality, especially in summer months when the meteorological conditions in the Mediterranean contribute to the formation of photochemically generated secondary pollutants and their accumulation in the lower tropospheric layers (Marmer and  
355 Langmann, 2005; Contini et al., 2011; Merico et al., 2021). Ship diesel engines are strong emitters of both primary and secondary PM. Primary PM in diesel are mostly emitted as ultra-fine particles and include soot, ash and a variety of organics as polycyclic aromatic hydrocarbons. Shipping secondary PM emissions include  $\text{SO}_4^{2-}$ ,  $\text{NO}_3^-$  and organics (Gobbi et al., 2020). From previous studies using high temporal resolution particle measurements at three sites on the coast of Venice, the mixing time of typical pollution plumes from ships with the surrounding air is between 20 minutes and one hour (Contini et al., 2011;  
360 Merico et al., 2021). This transport is confirmed by the COSMO wind direction and speed (see Fig. 6 and Fig. S9.2 in the supplement) at 12:00 UTC on 20 July 2017, that indicate SE (sea-land breeze) prevailing winds up to an altitude of 200 m, whereas SW winds were found to predominate between 500 m and 2000 m.



365 **Figure 7:** Vertical distribution of CO, O<sub>3</sub>, SO<sub>2</sub> and NO observed during the first (left; waypoints 6a to 6e) and second (right; waypoints 6f to 6j) shuttles during E-EU-06 on the 20.07.2017.



As anticipated, the measured values of CO, SO<sub>2</sub>, NO<sub>2</sub>, NO<sub>y</sub>, HCHO, C<sub>3</sub>H<sub>6</sub>O, O<sub>3</sub>, rBC, NO<sub>3</sub><sup>-</sup>, SO<sub>4</sub><sup>2-</sup>, and OA were all significantly less during the southern part (**X – F**) of the leg at 1630 m asl compared to the northern part (**G – X**). In contrast, 370 concentrations at 520 m asl were all similar (or significantly greater for HCHO) in the south (**X – F**) compared to the north (**G – X**) part of the leg. Particularly high HCHO/NO<sub>2</sub> ratios (ranging from ~9 to 10) resulting from particularly low NO<sub>2</sub> concentrations were observed at 1630 m asl, indicative of an aged pollutant plume. Backward trajectories indicate similar air 375 mass origin to those observed further north (**G-X**) in the same leg, albeit not passing lower than ~1200 m asl, whereas at 520 m asl they indicate a slow motion of air masses from ground level around 45.0 °N, 12.0 °E during the previous 12 hours. The air motion was therefore noticeably different between the BL at 520 m and the FT at 1620 m asl. HYSPLIT estimations indicate 380 that the contribution of CO emissions from the Po Valley to the CO enhancement at 520 m asl (~8 ppb) was primarily due to emissions within the last 6-24 hours, with no significant contribution from more recent emissions, i.e., different again from what was computed for 1630 m asl.

The comparison of the two shuttles shows similar mixing ratios at 3150 m above the GV for all species. Mixing ratios were 385 much more variable at 1630 m asl where plumes of pollutants originating within the BL in the CPP (6b-6c) or in the FT (approaching 6i) and traveling eastward were probed. In these polluted layers the highly processed probed air is reflected in the NO<sub>y</sub> to NO<sub>2</sub> ratio being on average a factor of ~3 to 4 higher than that in the BL.

The chemical processing of emissions during mixing is affected by the ambient air conditions. In the lower FT (1600 – 2000 m), the relative humidity was higher than at the ground, and H<sub>2</sub>O mixing ratio increased with altitude. Under high humidity 390 conditions, transformation of NO<sub>x</sub> compounds to HNO<sub>3</sub> and subsequent conversion to aerosol phase is favored (e.g., Guimbaud, 2002). Nitrate production in the entrainment zone of the BL has been previously documented in the area of Milan in summer (Curci et al., 2015). Based on WRF-Chem simulations at the regional scale, Curci et al. (2015) showed that chemistry and dynamics are strongly interlinked in the NO<sub>y</sub> spatial variability over the whole Po Valley and Northern Adriatic in July. In particular, the rate of nitrate production is higher in the upper BL, where RH is above the ammonium nitrate deliquescence point (~ 60 % RH, Talbot et al, 2016), which was the case at the points where NO<sub>y</sub> and NO<sub>3</sub><sup>-</sup> enrichments were 395 observed by HALO. Interestingly, the HYSPLIT simulations do not capture the increase in CO observed at around 1600 m, which may have a BB origin given the number of active fires at the time of the measurements and the high HCHO and CO mixing ratios observed. The polluted layer at this altitude may be a returning layer of pollution transported from inland to the coast as the result of combined breezes reinforced by upslope winds. This behaviour has been observed in other coastal areas (McKendrey and Lundgren, 2000; De Wekker and Kossman, 2015). The air masses in the sea breeze travel inland during the morning and early afternoon by incorporating weaker upslope circulatory cells (e.g., Millán et al., 2004). The mountain slopes act as convective-orographic chimneys that link the surface flows directly with their return flows aloft and lead to vertical recirculations of differently aged pollutants emitted along the coasts for several days. The decrease in mixing ratios observed around 10:50 UTC between waypoints 6h and 6i indicates the extension of this return layer.

400

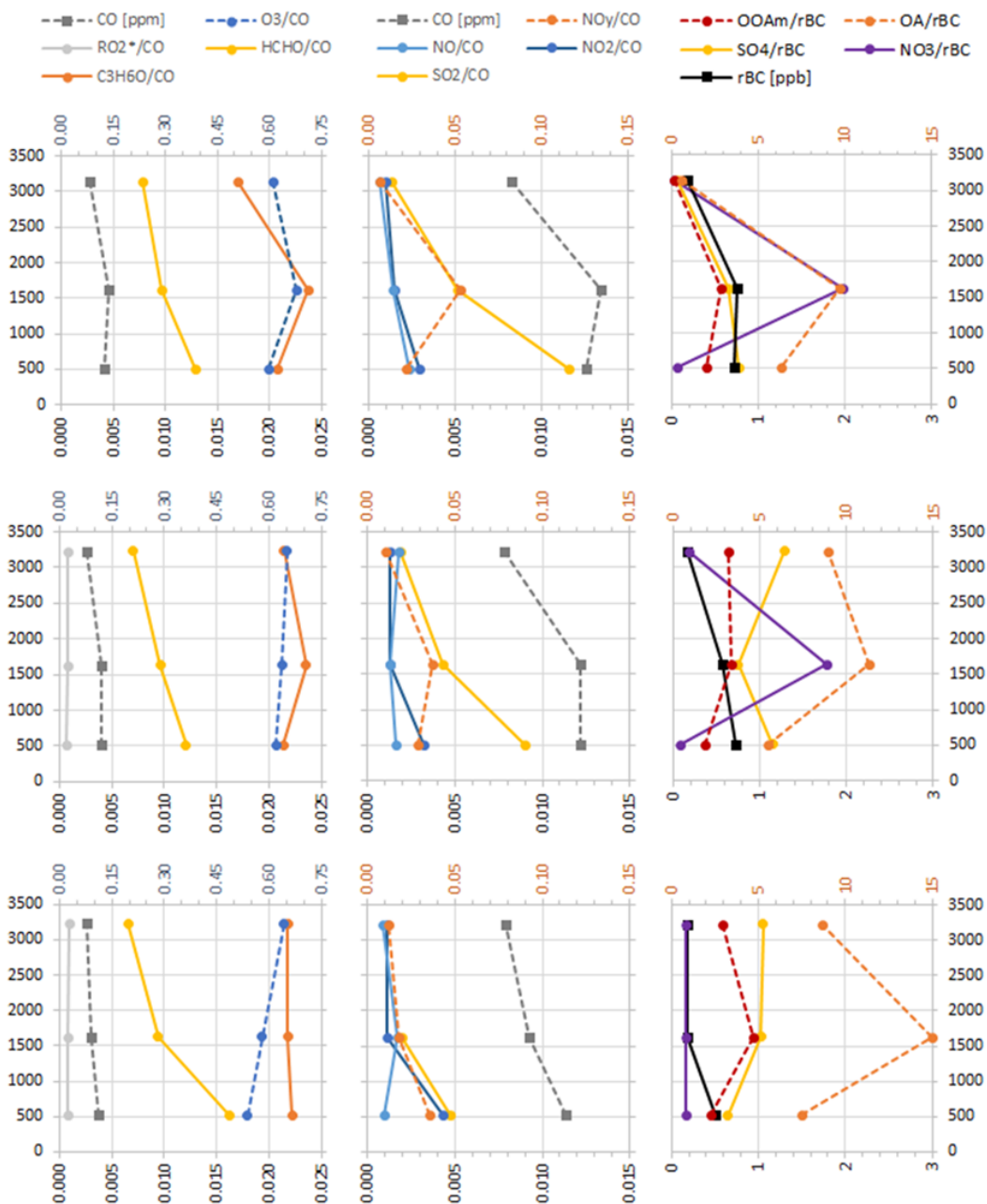


**Figure 8: Profiles of CO (ppm) and rBC (ppb), and ratios between selected species between B and C (top), G and X (middle) and X and F (bottom) in the GV. See Fig. 3 for the position of B, C, F, G and X. Dashed lines refer to the top x-axis.**

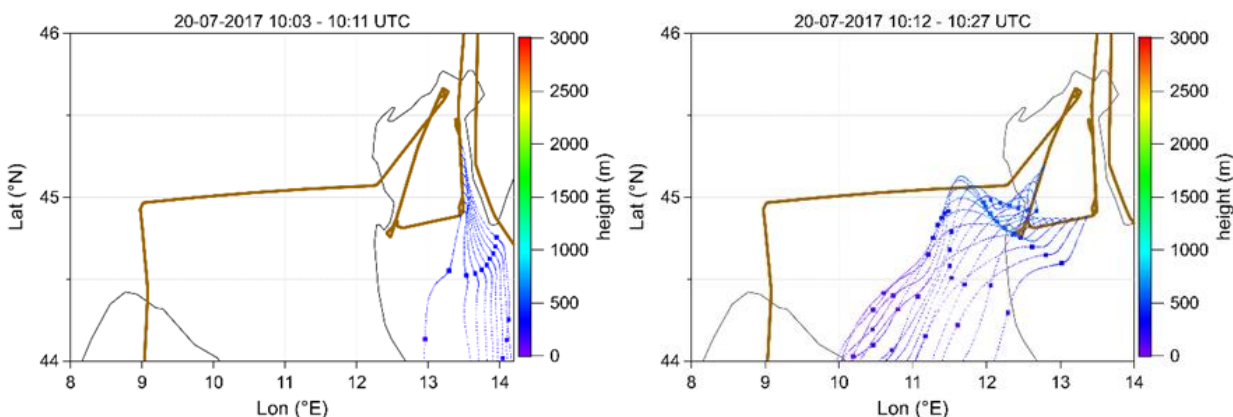
3) Transect in the marine BL across the Adriatic Sea.

405 During the westwards transect at 520 m asl from **B** to **F** (6e to 6f), a pollution plume was probed between 10:12 and 10:18 UTC with CO mixing ratios greater than 130 ppb. This plume was characterised by significant increases in CO, HCHO, C<sub>3</sub>H<sub>6</sub>O,



O<sub>3</sub>, NO<sub>2</sub>, NO<sub>y</sub>, NO<sub>3</sub><sup>-</sup>, and OA compared to the previous transect along the Adriatic coast at 520 m asl (6d-6e). Increases in NO<sub>y</sub>/CO, C<sub>3</sub>H<sub>6</sub>O /CO, NO<sub>y</sub>/NO<sub>2</sub>, ratios were also significant, pointing to a photo-chemically processed air mass. HYSPLIT simulations suggest a 20 ppbv enhancement in CO due to emissions from the Po Valley primarily during 6 to 48 hours prior 410 to the measurements. Backward trajectories confirm a slow motion to the sampling point of air masses circulating below 500 m agl over the CPP between approximately 45.2°N – 45.8°N, and 10.4°E – 11.6°E, an area including Brescia and Verona urban areas, where particularly high NO<sub>x</sub> concentrations were measured at the ground (see Section 3.2). This plume represents an example of a “smog” plume from the CPP being exported eastwards over the Adriatic Sea. Notably, the HCHO/NO<sub>2</sub> ratio being 4.1 indicates that O<sub>3</sub> photochemical production was NO<sub>x</sub>-limited at the time and location of the measurements.

415 A second pollution peak (CO = 135±6 ppbv) was probed at the end of this transect around waypoint 6f. Mixing ratios and ratios of the mixing ratio of different species were not significantly different from those in the previous plume, except for the NO mixing ratio and NO/CO ratio, which were about twice as high, indicating a larger contribution of fresh emissions. This was confirmed by HYSPLIT simulations showing a significant contribution of 3-6 hr old emissions from the Po Valley to ΔCO. In contrast with the previous plume, backward trajectories indicate stagnant air masses for the previous 6 hours, and 420 contact with the surface at ~45.0°N, 12.1°E (i.e., near Venice) about 12 hr before the measurements. NO and SO<sub>2</sub> peaks at 6f (520 m asl) could be associated with fresh local surface emissions. A significant contribution to air pollution of shipping and industrial activities around the port of Venice is consistent with the significant contribution of recently emitted air masses (3-6 hr age) to the 20 ppb CO enhancement of Po Valley origin computed by HYSPLIT (see e.g., waypoint 6f in contrast to 6e).



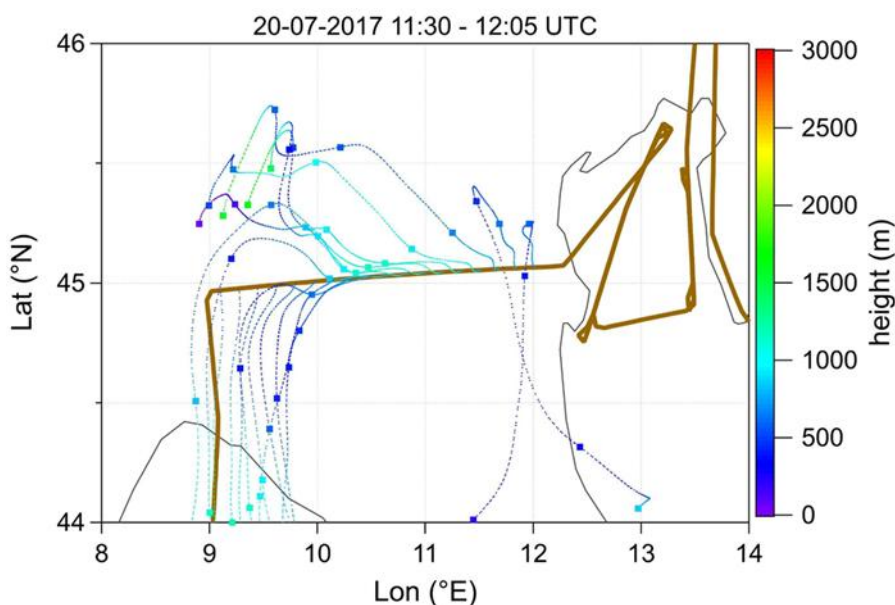
425

**Figure 9:** Twenty four hours FLEXTTRA backward trajectories calculated for E-EU-06 on 20 July. The trajectories are started each minute at the HALO altitude within the time intervals indicated on the top of each graph. Dots mark the 6h time steps along each trajectory. The flight track is shown in brown.



430 **3.1.2 Distribution of pollutants in the BL across the central Po Plain (CPP)**

HALO flew within the BL at 840 m between 11:25 and 12:07 UTC (waypoints 61-6m). The wind field simulations at the HALO flight altitude of  $840\text{ m} \pm 200\text{ m}$  evidence the difficulties in exactly assigning the origin of the air masses in this flight transect. According to COSMO simulations (see Sect. 9 in the supplement), there was a light breeze (wind speed  $< 2\text{ ms}^{-1}$ ) with a SW component above 1200 m within the BL during the E-EU-06. The FLEXTRA trajectories indicate that the probed air 435 masses mostly travelled across the CPP (see Fig. 10). However, the accuracy of the trajectories is limited by the prevailing low wind conditions during the E-EU-06 flight. This is demonstrated by perturbing the starting point of the COSMO-LAGRANTO backward-trajectories on 20 July 2017 horizontally within a radius of 2000 m and vertically by  $\pm 200\text{ m}$  around the real location and altitude of HALO, respectively (see the sensitivity study in Sect. S10 in the supplement). Both COSMO 440 and LAGRANTO SW flows at the top and above the BL are compatible with a SW synoptic scale circulation also transporting some desert dust (see Sec 3.4 and S13 in the supplement). Furthermore, the results indicate that slow horizontal and vertical mixing resulted in a poorly or slowly mixed BL. This is further discussed in Sect. 3.3.



445 **Figure 10:** Twelve hours FLEXTRA backward trajectories calculated for E-EU-06 on 20 July when overpassing the CPP. The trajectories are started each minute at the HALO altitude within the time interval indicated on the top of the graph. Dots mark the 6h time steps along each trajectory. The flight track is shown in brown on the map.

Selected mixing ratios of different species and ratios of mixing ratios obtained from airborne measurements during such east to west transect above the CPP are shown in Fig. 11. HCHO/NO<sub>2</sub> ratios ranging from 1 to 4 were the lowest observed during the whole E-EU-6 flight, and indicate that the O<sub>3</sub> photochemical production regime could not be safely qualified as NO<sub>x</sub>- or VOC-limited.



450 The variations in the concentrations of the species observed are highlighted by averaging measurement data over 8 different periods (P) lasting ~2 to 11 minutes (i.e., 16 to 80 km), primarily defined on the basis of CO variations, which are used as an indicator of ground-based pollution source emissions (see vertical red lines in Fig.11). Three of these periods: P2 (11:32-11:35 UTC), P5 (11:43-11:52 UTC) and P8 (12:03-12:07 UTC) with CO mixing ratios  $\leq 110$  ppbv were defined as local and temporary background. In these 3 periods, comparatively lower  $\text{SO}_2$ , NO,  $\text{NO}_2$ ,  $\text{NO}_y$  mixing ratios and  $\text{NO}_3^-$ , OA, and rBC mass concentrations were observed (see Fig.11). The HYSPLIT computed contributions of emissions from the Po Valley to measured CO mixing ratios dropping from 20 ppbv during period P2, to 5 ppbv and 2 ppbv during periods P5 and P8, respectively, suggest that the causes for the relatively low CO values observed during these 3 periods were probably different. During period P1 between 11:26 and 11:32 UTC (from  $12.33^\circ\text{E}$  to  $11.83^\circ\text{E}$ ), CO mixing ratios  $>110$  ppbv (average =  $130 \pm 5$  ppbv) were measured quasi continuously. However, no significant enhancements in gaseous or particulate species with respect to CO and rBC, respectively, were observed during this period (see histogram in Fig.12). NO/CO and  $\text{NO}_2/\text{CO}$  ratios were even significantly lower than in the periods defined as background. Backward trajectories suggest that sampled air masses travelled slowly in the BL from below 500 m agl around the CPP centre ( $44.5^\circ\text{N}$ - $45.5^\circ\text{N}$ ,  $10^\circ\text{N}$ - $11^\circ\text{E}$ ) during the previous 24 hours (Fig. 10). HYSPLIT simulations also indicate a large contribution ( $\sim 20$  ppbv) of local emissions primarily during the past 6 to 48 hours to the measured CO mixing ratios. The composition of the air sampled during P1 is probably representative 460 for the mid-day CPP regional pollutant mix. Low  $\text{NO}_y/\text{CO}$ ,  $\text{NO}_3^-/\text{rBC}$  and  $\text{OOAm}/\text{rBC}$  ratios suggest that this air mass was not much processed.

Period P3 between 11:36 and 11:39 UTC (from  $11.50^\circ\text{E}$  to  $11.26^\circ\text{E}$ ) was characterised by increases in  $\text{SO}_2$ , NO,  $\text{NO}_y$ , and particulate species (except  $\text{SO}_4^{2-}$ ), but cannot be further analysed due to the lack of simultaneous measurements of CO and nitrogen oxides during most of the period.

470 During period P4 (11:40 – 11:43 UTC) from  $11.14^\circ\text{E}$  to  $10.94^\circ\text{E}$ , CO mixing ratios averaged  $129 \pm 4$  ppbv. Increases in NO,  $\text{NO}_2$ ,  $\text{NO}_y$ ,  $\text{NO}_3^-$ ,  $\text{SO}_4^{2-}$ , OA and rBC were observed. However, only  $\text{NO}_y/\text{CO}$  and  $\text{NO}_3^-/\text{rBC}$  were significantly larger while  $\text{HCHO}/\text{NO}_2$  ratios were lower than in the so-called background periods. FLEXTRA backward trajectories (Figure 10) indicate air masses coming from the BL in the CPP (around  $45.5^\circ\text{N}$ ,  $9.5^\circ\text{E}$ ) about 18 hours before. These observations indicate that the probed air masses resulted from the processing of originally  $\text{NO}_x$  rich emissions (e.g. from traffic). However, HYSPLIT 475 calculates only a 10 ppbv CO increment coming from emissions in the Po Valley, primarily emitted 6-24 hours prior to the measurements.

In contrast, Period P6 (11:53 – 11:57 UTC) between  $10.03^\circ\text{E}$  and  $9.72^\circ\text{E}$  ( $\text{CO} = 120 \pm 2$  ppbv) is primarily characterised by increases in  $\text{NO}_2$  and  $\text{SO}_2$  mixing ratios. While  $\text{NO}_2/\text{CO}$  ratios were on average not significantly larger than during the background P5 period,  $\text{SO}_2/\text{CO}$  ratios reached the maximum mean value (0.017) observed over the CPP. Backward trajectories 480 indicate that air masses travelled in the BL around Genoa (approx.  $44.5^\circ\text{N}$ ,  $9^\circ\text{E}$ ) about 12 hours prior to the measurements, i.e. a drastic shift in air mass origin compared to Period P4 is found. According to HYSPLIT, the  $\Delta\text{CO}$  contribution of emissions



from the Po Valley to the CO observed is less than 3 ppbv, and about half of this increase occurred during the last 6 hours before the measurements.

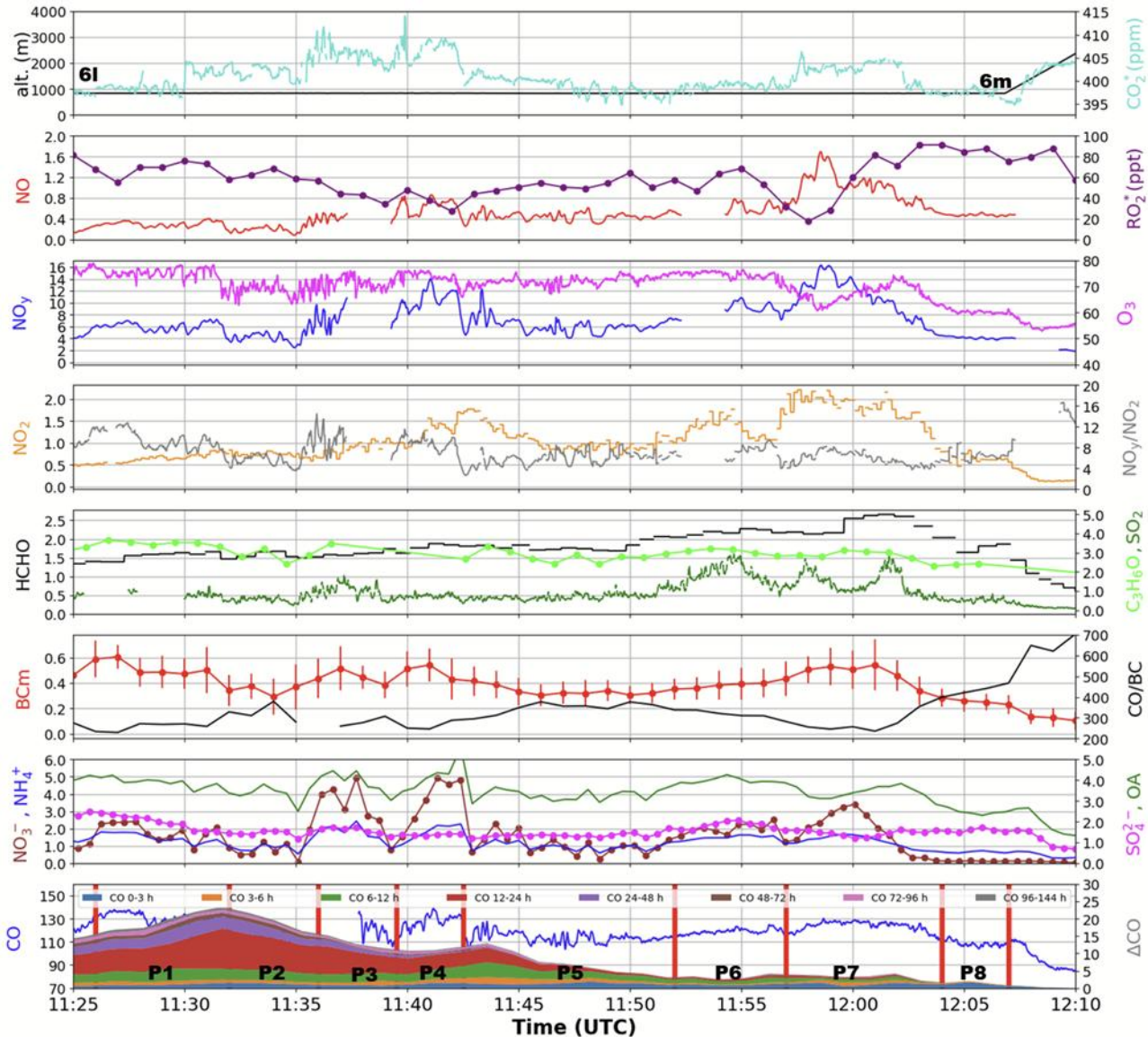


**Figure 11:** Temporal variation of NO, NO<sub>2</sub>, NO<sub>y</sub>, O<sub>3</sub>, CO, HCHO, C<sub>3</sub>H<sub>6</sub>O, SO<sub>2</sub>, RO<sub>2</sub><sup>\*</sup>, and rBC, NO<sub>3</sub><sup>-</sup>, NH<sub>4</sub><sup>+</sup>, SO<sub>4</sub><sup>2-</sup>, and OA (in  $\mu\text{gm}^{-3}$  STP) observed on board HALO over the CPP during EMeRGe E-EU-06. The mixing ratios are in ppb if not indicated otherwise. HCHO and NO<sub>2</sub> values are retrieved from miniDOAS measurements. The flight altitude and the changes in course and altitude (waypoints 6m-6n) are marked in the top panel. The NO<sub>y</sub>/NO<sub>2</sub> ratio is also shown. In the bottom panel HYSPLIT simulations of the contribution of Po Valley emissions ( $\Delta\text{CO}$ ) in different aged air masses to the observed CO (in blue) are shown. Vertical red lines marked the time intervals selected for the analysis (P1-P8, see text).



High  $\text{SO}_2/\text{CO}$  emission factors are characteristic of emissions from ships and refineries, which use higher sulphur -content fuels compared to e.g. road transport. Potential emission sources in the GG are the port of Genoa, a large European port 495 involved in sea freight import-exports having a substantial amount of maritime traffic (APICE, 2009; Marmer and Langmann, 2005), its surroundings, and the refinery IPLOM in Busalla (<https://iplom.it/>,  $44^{\circ}34'54''\text{N}$ ,  $8^{\circ}56'29''\text{E}$ ).

During P7 (11:58-12:02 UTC,  $\text{CO} = 126 \pm 2 \text{ ppbv}$ ) from  $9.62^{\circ}\text{E}$  to  $9.25^{\circ}\text{E}$ , the highest  $\text{NO}$ ,  $\text{NO}_2$ ,  $\text{NO}_y$ , and  $\text{HCHO}$  mixing 500 ratios of all transects in the BL over the CPP were measured. Two  $\text{SO}_2$  peaks were also observed at the beginning and the end of the period. In contrast, peaks in particulate species such as  $\text{rBC}$  and  $\text{NO}_3^-$  were similar or lower than in the other pollution plumes.  $\text{NO}/\text{CO}$ ,  $\text{NO}_2/\text{CO}$  and  $\text{NO}_y/\text{CO}$  ratios were significantly higher than during the background periods, pointing to a mixture of fresh and aged emissions from combustion sources.  $\text{HCHO}/\text{NO}_2$  ratios were significantly lower, and the lowest observed over the CCP (1.3), getting close to the threshold indicating a VOC-limited  $\text{O}_3$  production regime. The  $\text{O}_3/\text{CO}$  was significantly lower than in background conditions, and also the lowest observed over the CPP, indicating the titration of  $\text{O}_3$  by 505  $\text{NO}$  as additionally indicated by the  $\text{NO}$ ,  $\text{O}_3$ , and  $\text{RO}_2^*$  observations. The two peaks in  $\text{SO}_2/\text{CO}$  suggest that ship or refinery emissions were partially sampled. The advection of coastal emissions inland is confirmed by backward trajectories passing in 510 the MBL over the GG within 12 hours before the measurements, and by the HYSPLIT estimate of  $\sim 50\%$  contribution of fresh emissions ( $< 6\text{hrs}$ ) to the  $\Delta\text{CO}$  from the Po Valley.

### 3.1.3 Vertical distribution and advection of pollutants in the Gulf of Genoa (GG)

HALO flew southwards from waypoint 6m ( $44.86^{\circ}\text{N}$ ,  $8.97^{\circ}\text{E}$ , 840 m asl) to waypoint 6n ( $44.63^{\circ}\text{N}$ ,  $9.04^{\circ}\text{E}$ , 2590 m asl) 510 between 12:06 and 12:10 UTC.  $\text{CO}$ ,  $\text{SO}_2$ ,  $\text{NO}_2$ ,  $\text{NO}_y$ ,  $\text{RO}_2^*$ ,  $\text{O}_3$ ,  $\text{rBC}$ ,  $\text{OA}$ ,  $\text{OOAm}$ , and  $\text{SO}_4^{2-}$  values significantly decreased during the ascent, while the  $\text{NO}_3^-$  concentration did not significantly change and remained around  $0.06 \mu\text{gm}^{-3}$  STP.  $\text{NO}$  data were not available most of this period. Across the southward transect at 2590 asl between waypoints 6n and 6o ( $44.14^{\circ}\text{N}$ ,  $9.05^{\circ}\text{E}$ , 2590 m asl), mixing ratios of all species remained low and little variable.  $\text{RO}_2^*$  remained around  $45 \pm 13 \text{ pptv}$  (Table S8 in the supplement).  $\text{HCHO}/\text{NO}_2$  ratios were constantly greater than 4, characterising a  $\text{NO}_x$ -limited photochemical  $\text{O}_3$  515 production regime. According to HYSPLIT simulations, the contribution of sources located in the Po Valley to  $\Delta\text{CO}$  was null. There is no evidence that the air probed across this transect had recent contact with dry land for the previous 96 hours, air masses travelling above 2000 m asl parallel to the French south coast coming from the Iberian Peninsula via the Balearics. During this transect above GG (upwind of the CPP) at 2580 m asl,  $\text{NO}_2$ ,  $\text{NO}_y$ , and  $\text{O}_3$  mixing ratios were higher than above 520 GV (downwind of the CPP) at 3200 m asl, while the values of  $\text{CO}$ ,  $\text{NO}$ ,  $\text{SO}_2$ ,  $\text{HCHO}$ ,  $\text{C}_3\text{H}_6\text{O}$ , and the particulate species ( $\text{NO}_3^-$ ,  $\text{SO}_4^{2-}$ ,  $\text{rBC}$ ,  $\text{OA}$ ,  $\text{OOAm}$ ) were not significantly different. This means that on 20 July 2017 the CPP area was not a source of pollution in the FT above 2500 m asl.

The  $\text{NO}_y/\text{CO}$  ratio computed from E-EU-06 measurements remains between 0.03 and 0.12 within the BL. Above the BL, the concentration of both species decreases and their ratio remains around 0.01 at 2500 m in E-EU-06 and at 3000 m in E-EU-03.



Apart from reflecting the shorter lifetime of  $\text{NO}_y$ , this indicates the significance of additional long-range transport of CO in  
 525 the upper levels eastwards from the south of France during both HALO flights.

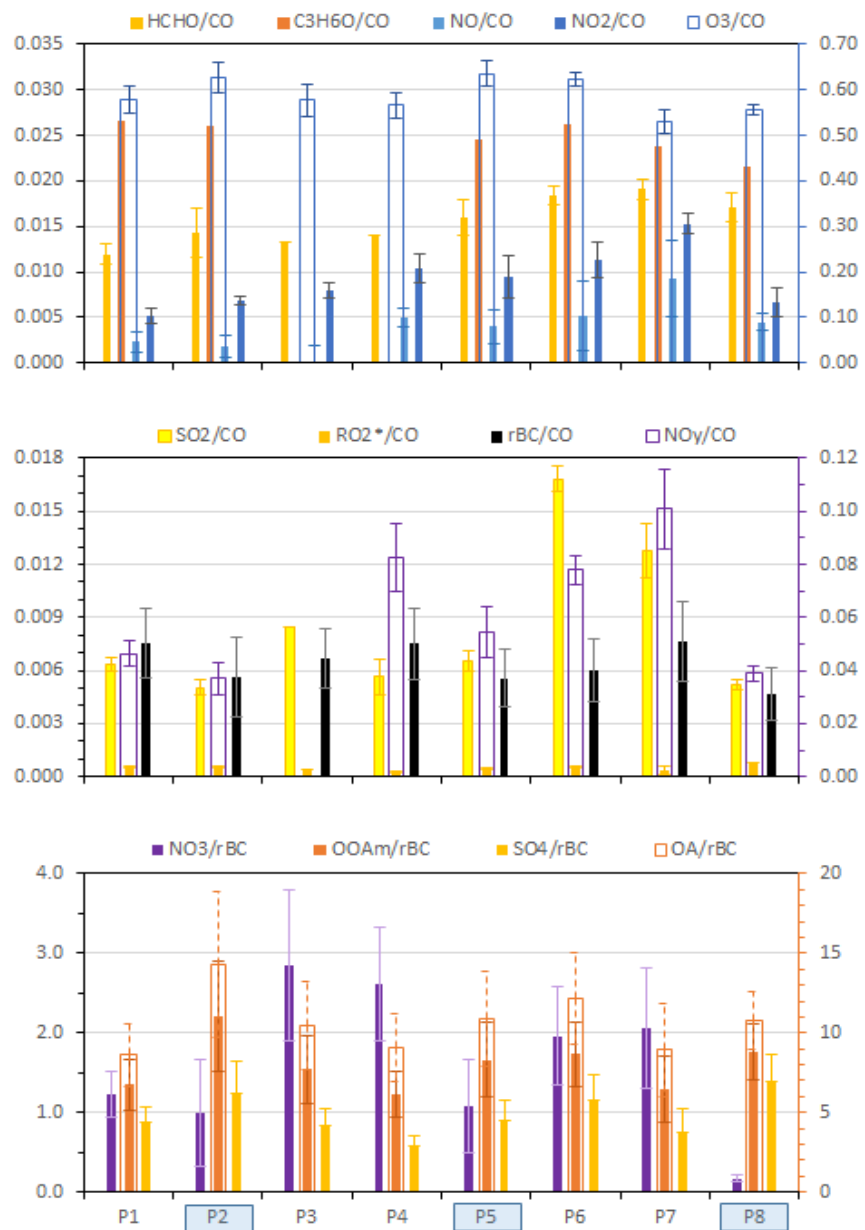


**Figure 12:** Ratios between selected species measured along the transect over the CPP at 830-840 m asl. Open bars refer to the right hand y-axes. Periods defined as background are highlighted in blue in the x axis. The delimiting times are marked in Fig.10 as red lines in the bottom panel



530 **3.2 Comparison of ground and airborne observations over the Po Plain**

As presented above, the mixing ratio and variability of the trace constituents investigated during the HALO flights were mostly higher in the BL than in the lower FT. This is expected as emission sources in the PP are predominantly at the ground, and convective and advective mixing in the BL may be relatively slow. The transport and dilution of pollutants in the BL along the Po Plain was further investigated by comparing the variability and distribution at the surface with the airborne observations 535 performed in the BL on the 20 July 2017. The NO<sub>x</sub>, CO, O<sub>3</sub> and SO<sub>2</sub> measured with 1hr resolution at the ARPA AQMN stations at altitudes between 10 m and 250 m asl. (see Table S6.1 in the supplement) in the proximity of the track were used for this purpose. Vertical and horizontal gradients of pollutants are expected to depend on the efficiency of the mixing within the BL. If the time scales are shorter for the horizontal than for the vertical mixing within the BL the distribution of trace gases above 540 the surface may not reflect the allocation of the emissions at the ground but be more homogeneous over larger areas in the upper layers. Short-lived species may react completely before mixing by small-scale turbulent motions that consequently affect the production of secondary pollutants such as O<sub>3</sub>.

Looking at the Po Plain as a whole, it appears that the largest CO mixing ratios (300 – 500 ppbv) were observed at traffic sites (7, 13, 16, 17), with the exception of the traffic site 6, while the lowest (100 – 200 ppbv) were generally observed at rural and 545 urban background sites (2, 3, 4, 15, 19, 23), with the exception of rural background site 10 (Fig.13). Note that according to Figure 5, the station 10 at 250 m asl is potentially under the influence of the transport of pollution of coastal origin. The observed CO distribution roughly reflects the distance of each site to major combustion sources, i.e., predominantly road traffic in summer. CO mixing ratios measured at ~800 m above the CPP (120 ± 8 ppbv) are not significantly different from those measured at 520 m asl in GV (126 ± 15 ppbv), and are independent from the CO mixing ratios measured at the ground stations, which were flown over (100 – 400 ppbv). This might be explained by the large contribution of long-range transported CO to 550 the mixing ratios in the BL at 800 m above the ground. According to HYSPLIT simulations, emissions from the Po Valley actually accounted at the maximum for 15 % to the CO mixing ratios measured on-board the aircraft.

Regarding NO<sub>x</sub>, extreme concentrations (30 – 60 ppbv) were observed at traffic sites 13 and 16, while moderate mixing ratios (10-12 ppbv) were measured at traffic sites 6 and 8. The higher degree of processing of the probed air masses is consistent with the significantly higher NO<sub>2</sub> than NO<sub>x</sub> ratios (i.e., higher NO<sub>2</sub> to NO content) at the stations 12-16.

555 Lower values (5-10 ppbv) were observed at regional background sites. Unlike CO, mean NO<sub>x</sub> mixing ratios were significantly greater at ~800 m above the CPP (1.4 ± 0.5 ppbv) compared to 520 m asl in GV (0.7 ± 0.1 ppbv), but 4 to 10 times less than at the air quality monitoring stations (5 – 15 ppbv), which were flown over, with no significant correlation between the ground level and aircraft altitude mixing ratios.

The lower horizontal variability in NO<sub>2</sub> measured in the BL at ~800 m agl compared to ground-level stations suggest again 560 road traffic as the major NO<sub>x</sub> source in the CPP in summer. Based on the mean vertical wind speed measured at the aircraft during the 6l-6m leg (0.07 m s<sup>-1</sup>), and a lower limit estimate of 3 hr for NO<sub>x</sub> lifetime (Valin et al., 2013), the decrease in NO<sub>x</sub> mixing ratio between the ground and the aircraft altitude could be estimated to a factor of ~3 only. Note that the measured



vertical wind speed would result in a BL mixing time of ~4-6 hr, i.e. the upper limit of the range for a convective BL between 20-30 min to a few hours (e.g. Maclean et al., 2017; Helbig et al, 2021). The significantly lower NO and NO<sub>2</sub> mixing ratios measured on board HALO than at the ground around 11:30 – 12:00 UTC on 20 July 2017 (Figure 13) indeed suggest a partial and incomplete mixing of the atmospheric BL between the ground and the aircraft altitude (~800 m agl), and/or an effective processing of local short-lived NO<sub>x</sub> emissions to unreactive products during slow mixing.

The range of the 1h-mean O<sub>3</sub> mixing ratios at ground stations between 11:00 and 12:00 UTC is smaller (45 – 72 ppbv) than for CO and NO<sub>x</sub>. As expected, the highest mixing ratio was observed at the regional background station 23, where anthropogenic NO<sub>x</sub> and VOC have mixed upstream with biogenic VOC (primarily isoprene). However, there is no correlation between the type of site and O<sub>3</sub> concentrations across the whole Po Plain. O<sub>3</sub> mixing ratios in the CPP at ~800 m agl were significantly higher than at ground level (+ 8%). This may imply incomplete mixing with the NO<sub>x</sub> ground emissions at the time of the flight and/or O<sub>3</sub> photochemical production in O<sub>3</sub> precursor rich air rising up by convection.

### 3.3 General features in the processing of the air masses over the Po Plain

Based on the ground-based and airborne observations described in the previous sections, some general features were identified in the transport and processing of pollution within the complex Po Plain. Besides information about the O<sub>3</sub> formation potential of the air masses, the obtained data check the suitability of HYSPLIT and dispersion models to reproduce the observed pathways.

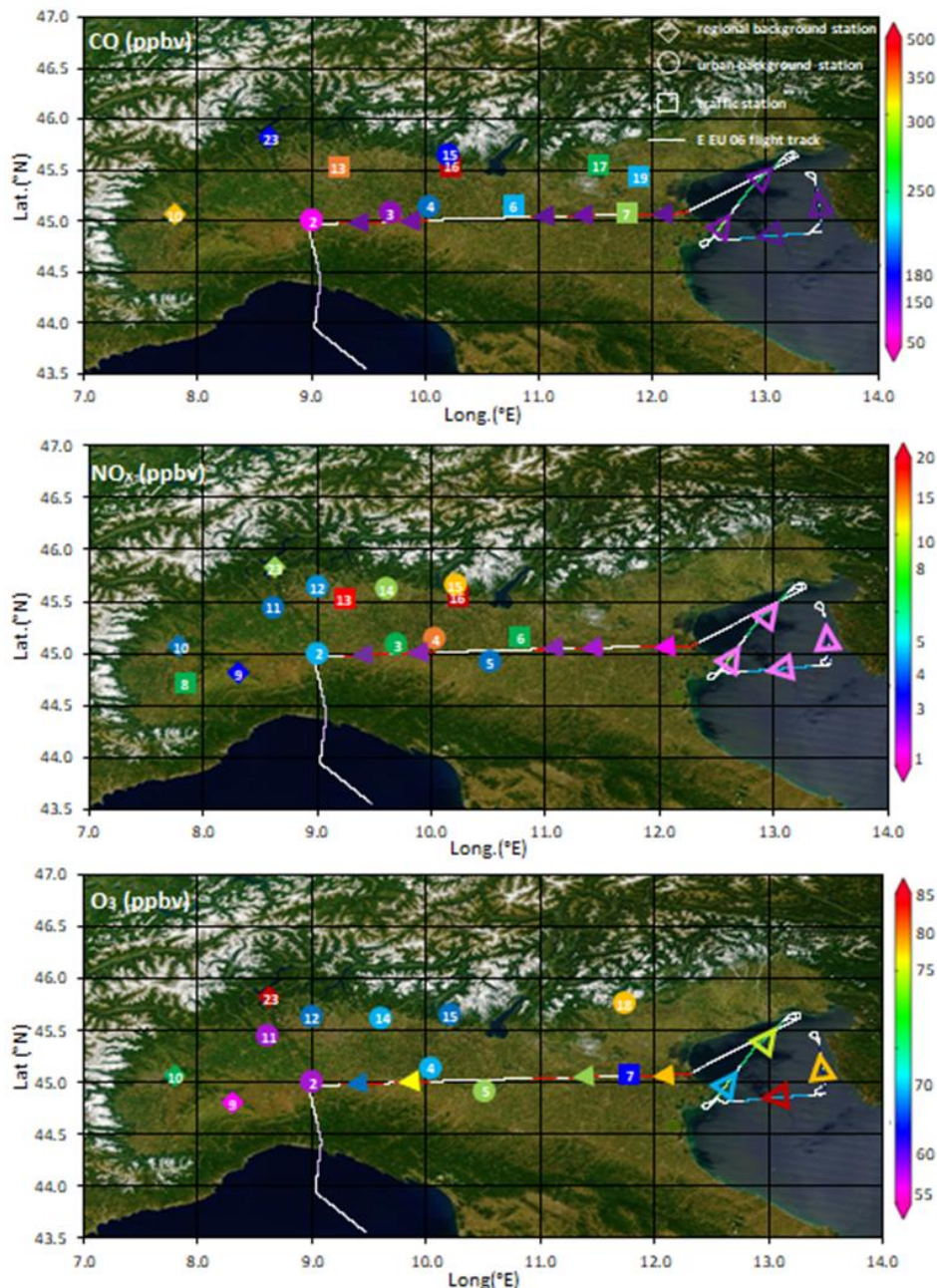
The air probed in GV was the most photochemically active. This resulted from the mixing of fresh emissions of primary pollutants with processed air masses, leading to the highest O<sub>3</sub> formation potential. The HCHO to NO<sub>2</sub>, HCHO to NO<sub>y</sub>, and NO<sub>y</sub> to NO<sub>2</sub> ratios were higher than in GG and CPP and indicated a NO<sub>x</sub> limited production of O<sub>3</sub>. The difference in HCHO/NO<sub>2</sub> ratios in the BL between GV and CPP is consistent with RO<sub>2</sub><sup>\*</sup> mixing ratios being about 20-50% higher in the former. The lower HCHO to NO<sub>2</sub> ratios detected anywhere else indicate a transition regime between NO<sub>x</sub> and VOC limited production of O<sub>3</sub> in the probed air masses with respect to the GV

The increase in NO to NO<sub>2</sub>, NO<sub>2</sub> to NO<sub>y</sub> and NO to SO<sub>2</sub> ratios in the GV transect was consistent with the increasing importance of fresh emissions in the transported air masses. The ratio between NO and SO<sub>2</sub> additionally indicated the mix of combustion processes responsible for pollution, primarily the sulphur content of the fuel burnt.

Concerning the origin of the sulphur compounds in the BL, port traffic and activities were identified as the major source of SO<sub>2</sub>. The highest SO<sub>2</sub>/CO ratios were observed during 3 transects at 520 m asl over GV (range = 0.008 – 0.012) and in the west of the CPP at 830-840 m asl (0.013). In the first case, the air masses had been transported in the BL above the Adriatic Sea during the previous 24 hours. In the western part of the HALO transect in the BL at ~800 agl above the CPP, the backward trajectories passed in the MBL over the port of Genoa in the GG within 12 hours before the measurements and a ~50% contribution of fresh emissions (< 6hr) from the Po Valley to ΔCO were estimated. SO<sub>2</sub> enhancements were not systematically accompanied by similar enhancements in SO<sub>4</sub><sup>2-</sup> as revealed by low SO<sub>4</sub><sup>2-</sup>/rBC ratios ranging between 0.8 and 1.4, probably due to the slow homogeneous oxidation of SO<sub>2</sub> to SO<sub>4</sub><sup>2-</sup> (characteristic time during day in summer ≈ a couple of days). High SO<sub>4</sub><sup>2-</sup>



/rBC ratios were observed during this measurement campaign in “background” conditions in the BL (up to 1.4, see sect. 3.1.2) and in the FT between 2600 and 3230 m asl (up to 2.3), which could also mask local photochemical  $\text{SO}_4^{2-}$  production.



600 **Figure 13:** Ground-based CO, NO<sub>x</sub>, and O<sub>3</sub> mixing ratios (colour scales) at traffic (square), urban background (circle), and regional background (diamond) stations of the ARPA and ACTRIS networks at the time of the E-EU-06 overpass. Station numbers refer to Table S6.1 in the supplement. Also shown are the mixing ratios measured along the aircraft E-EU-06 track (line) at 520 m asl over the GV (open triangles) and 830-840 m asl above the CPP (solid triangles)



The mean  $\text{NO}_y$  mixing ratio measured in the BL over the CPP was ~50% larger than over the coastal areas. This is explained not only by less BL venting and dilution in the CPP, but also by an effective processing of  $\text{NO}_x$ -rich emissions leading to e.g., 605  $\text{HNO}_3$  and  $\text{NO}_3^-$  production. This resulted in higher mean  $\text{NO}_y/\text{CO}$  and  $\text{NO}_3^-/\text{rBC}$  ratio in the CPP, albeit larger ratio punctually observed in the BL above GV. Similarly, increases in the  $\text{NO}_2/\text{NO}$  and  $\text{NO}_3^-/\text{NO}_2$  ratios were generally concurrent.

With regard to horizontal transport pathways, the observations indicate the contribution of fresh pollution advected from GG 610 in the CPP. This was in agreement with model-based wind fields and thus with the HYSPLIT simulations showing around a 50% contribution of the Po Valley emissions to CO emitted recently (<6hr age). However, the CO emissions from the Po Valley advected to the measurement points at the west tip of the CPP were estimated by HYSPLIT to be less than 5 ppb, i.e., 4% enhancement with respect to the total CO measured. This contribution is much lower than the 20% maximum enhancement 615 observed over the background periods (see detailed analysis in Sect. 3.1.1).

Furthermore, the comparison between HALO measurements performed at the lowest flight altitudes (about 800 m asl) over the CPP and at ground stations showed inhomogeneities in the vertical distribution of several species mixing ratios, especially 620 for CO and  $\text{NO}_x$ , and in less extension for  $\text{O}_3$ . Such inhomogeneities within the BL in urban areas with a complex distribution of emissions at the surface have already been addressed (Wang et al., 2021). Large eddy simulations suggest that the inefficient mixing of reactants such as e.g. NO and peroxy radicals can affect the production of secondary pollutants such as e.g.  $\text{O}_3$ , especially when the location of anthropogenic NO emissions and biogenic VOC emissions are separated. Simulations by Wang et al. (2022) showed that  $\text{O}_3$  significantly increased with altitude (20 ppbv) between 100 and 800 m agl above Hong Kong in 625 the polluted case (surface NO and  $\text{NO}_2$  of ~30 ppbv), but not in the “clean” case (+ 1 ppb between 100 and 800 m agl), where NO and  $\text{NO}_2$  mixing ratios at the ground were 0.5 and 3 ppb, respectively. In polluted conditions, they computed a decrease in the  $\text{O}_3$  photochemical production rate due to radical species segregation ranging from 50% at about 150 m to less than 20% above 500 m over the urban area of Hong Kong. The  $\text{NO}_x$  mixing ratios measured across the CPP on 20 July between 12:00 and 13:00 UTC ranged between the extremes of their simulations. Measured and simulated radiosondes indicate that turbulence 630 in the BL atmosphere over the CPP was even less than in the simulations of Wang et al. (2022). This may explain the small increase of  $\text{O}_3$  between the ground and 800 m agl over the CPP, and the drastic decrease in  $\text{NO}_x$  between these 2 levels. Hůnová et al. (2023) showed non-uniform  $\text{O}_3$  concentration gradients and temporal changes in air columns of 2-8 m, 8-50 m and 50-230 m from seven-year  $\text{O}_3$  measurements taken at four heights up to 230 m above the ground in a rural area in the Czech-Moravian Highlands.

635 Aged polluted layers were observed above the top of the BL in GV. The HYSPLIT simulations do not capture the increase in CO observed but assign a higher relative contribution of air masses being > 24-48 hours old than in the air within the BL below. This may corroborate them as returning pollution layers of previous days.  $\text{HCHO}/\text{NO}_2$  ratios were on average particularly high in these layers (~6 to 8), as compared to the BL underneath (~4 at 520 asl) and above the CPP (~2 at 830-840 asl), and well above the threshold (~4) above which  $\text{O}_3$  photochemical production is considered to be  $\text{NO}_x$ -limited.



### 3.4 Desert dust transport and secondary organic aerosol formation above the central Po Plain

Transport of desert dust to the Central Mediterranean and the Italian Peninsula is a frequent phenomenon, particularly in summer (Barnaba and Gobbi, 2004). It has important impacts on PM-air quality metrics (Pederzoli et al., 2010, Barnaba et al., 2022), as well as on the chemistry of the atmosphere, such as providing surface for heterogeneous reactions including  $O_3$  removal mechanisms from the gas phase (e.g., Zhu et al., 2010; Wang et al., 2017). Desert dust may also influence nitrate partitioning between gas and aerosol phase (e.g., Karydis et al., 2016), the heterogeneous formation of sulphate catalysed by iron (Itahashi et al., 2022) and the neutralization of acids such as  $HNO_3$  and  $H_2SO_4$  (e.g., Athanasopoulou et al., 2016).

The slow vertical mixing and low photochemical activity observed over the CPP on 20 July 2017 may be related to the presence of Saharan dust. In fact, elevated desert dust layers were observed by ground based remote sensing over the central Po Valley during the EMeRGe HALO flights (Andrés Hernández et al., 2022).

Figure 14 shows the complex aerosol stratification as observed on July 20 during the E-EU-06 HALO flight by the ALICENET ALC operating in Milan-Bicocca. Aerosol profiles from the lidar operating in Ispra at the time of the HALO overpass are reported in Fig. 15. The arrival of elevated, desert-dust layers over the CPP is documented to occur already the day before by the Milan ALC (see Figure S12.1 in the Supplement showing the continuous evolution of the aerosol vertical profiles during the whole EMeRGe campaign in Europe: 11-20.07.2017). This is also in agreement to predictions by the multi-model desert dust forecasts (Basart et al., 2019) made available by the Dust Regional Center (<https://dust.aemet.es/products/daily-dust-products>) and reported in Fig S13 in the supplement.

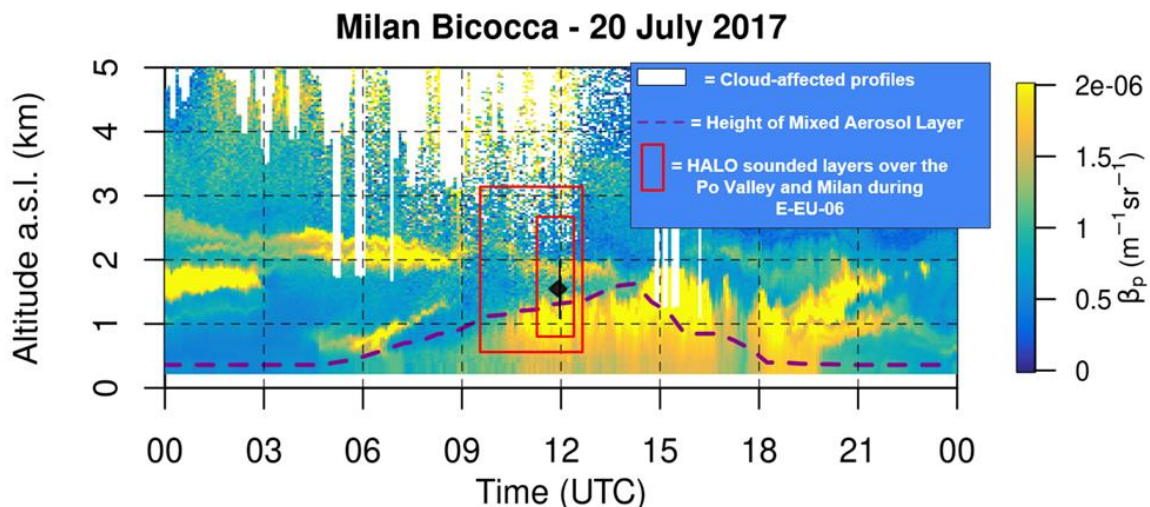
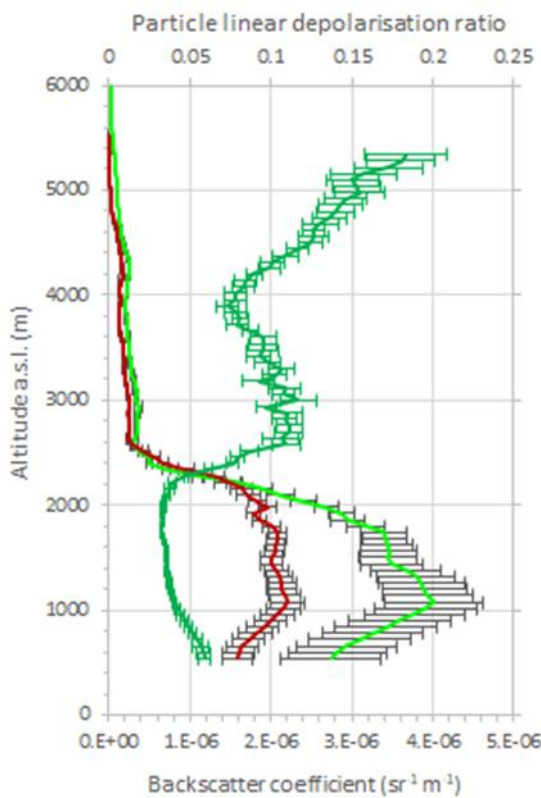


**Figure 14:** Continuous (0-24 UTC, x-axis) vertical profiles (0-5 km asl, y-axis) of aerosol backscatter at 1064 nm as observed by the ALICENET ALC system operating in Milan-Bicocca on July 20, 2017. Cloud-affected profiles are filtered out from the cloud base upwards (white areas). The height of the Mixed Aerosol Layer (MAL, dashed purple line), proxy of BLH, is derived from the Alicenet data processing (Bellini et al., 2024). BLH value derived at 12 UTC from radiosonde measurements in Milan is also reported (black diamond, see Table 1). Red boxes identify time-altitude windows sounded by HALO over the wider Po Valley (outer box) and Milan (inner box) areas.



660 In particular, elevated aerosol layers up to over 5000 m altitude are visible in the ALC and lidar traces (Fig. 14-15). The mineral  
dust nature of the particles is confirmed by the aerosol depolarization trace of the Ispra lidar, markedly increasing above 2500  
m. In the morning, clouds are observed to form above 3000 m within the dust layer. During E-EU-06, HALO actually flew 60  
km south of Milan and 90 km south of Ispra around 12 UTC at 830-840 m asl. Particle number size distributions measured on  
board HALO when closer to Ispra and Milan showed a distinct coarse mode at 1.5  $\mu\text{m}$ , similarly to what has been previously  
665 observed during the MINATROC campaign in a desert dust outbreak at Monte Cimone (Italy) in June-July 2000 (Van  
Dingenen et al., 2005). However, the contribution of coarse particles to the total particle number was limited (~1/10000)  
compared to what was previously measured (~2/1000).



670 **Figure 15:** Vertical profiles of the particle light backscatter coefficient at 1064 (red) and 532 (light green) nm (bottom x-axis), and  
the linear depolarization ratio (dark green, top x axis) at 532 nm measured by the aerosol Lidar in Ispra on the 20 July between  
11:01 and 13:01 UTC.

The number concentration of particles with diameters greater than 500 nm ( $\text{Nd} > 500\text{nm}$ ) in the free troposphere is used as a proxy for the dust number concentration (DeMott et al., 2010; Weger et al., 2018; Zhang et al., 2019). For heterogeneous reactions, the surface area concentration is the decisive quantity and will be denoted here as  $dS_{d>500\text{nm}}$ . The HALO observations  
675 (Fig. 16) indicate a larger amount of dust above GV at 1630 m asl ( $\sim 30 \mu\text{m}^2 \text{cm}^{-3}$ ), above GG at 2600 m asl ( $\sim 20 \mu\text{m}^2 \text{cm}^{-3}$ ), and in the western part of the transect above the CPP at 830-840 m asl ( $\sim 10 \mu\text{m}^2 \text{cm}^{-3}$ ), where air masses coming from GG



were advected. For comparison, the surface area due to the coarse mode observed in Monte Cimone (at 2165 m asl) in June-July 2000 was  $44 \mu\text{m}^2 \text{cm}^{-3}$  (Van Dingenen et al., 2005), but in that case the dust plume was more intense and vertically thick (reaching up to 8 km altitude, Gobbi et al., 2003) than the one sounded during EMeRGe.

680

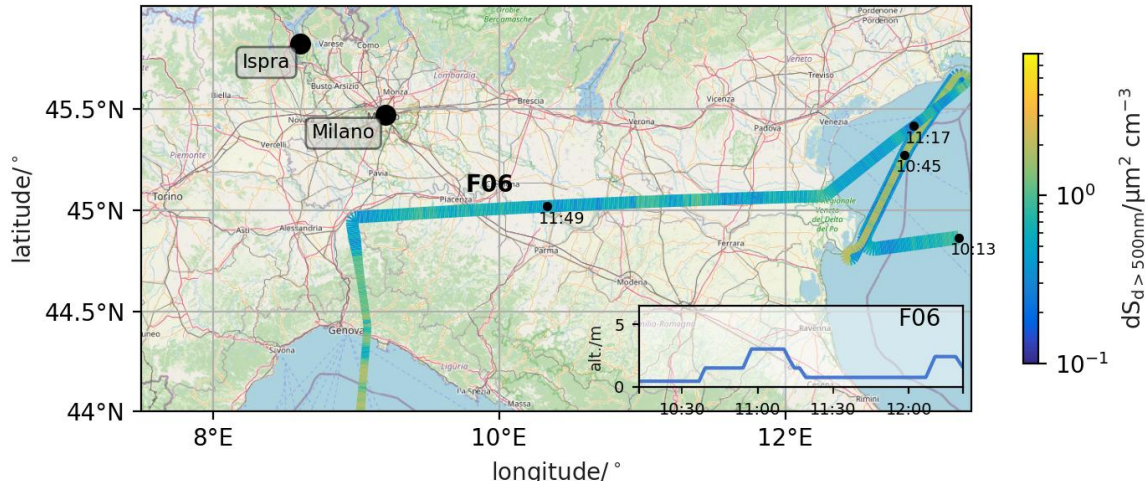


**Figure 16: Surface area concentration of particles with diameter larger than 500 nm measured by the optical particle counter on-board HALO along the flight track. Map data from OpenStreetMap, <https://www.openstreetmap.org/copyright>.**

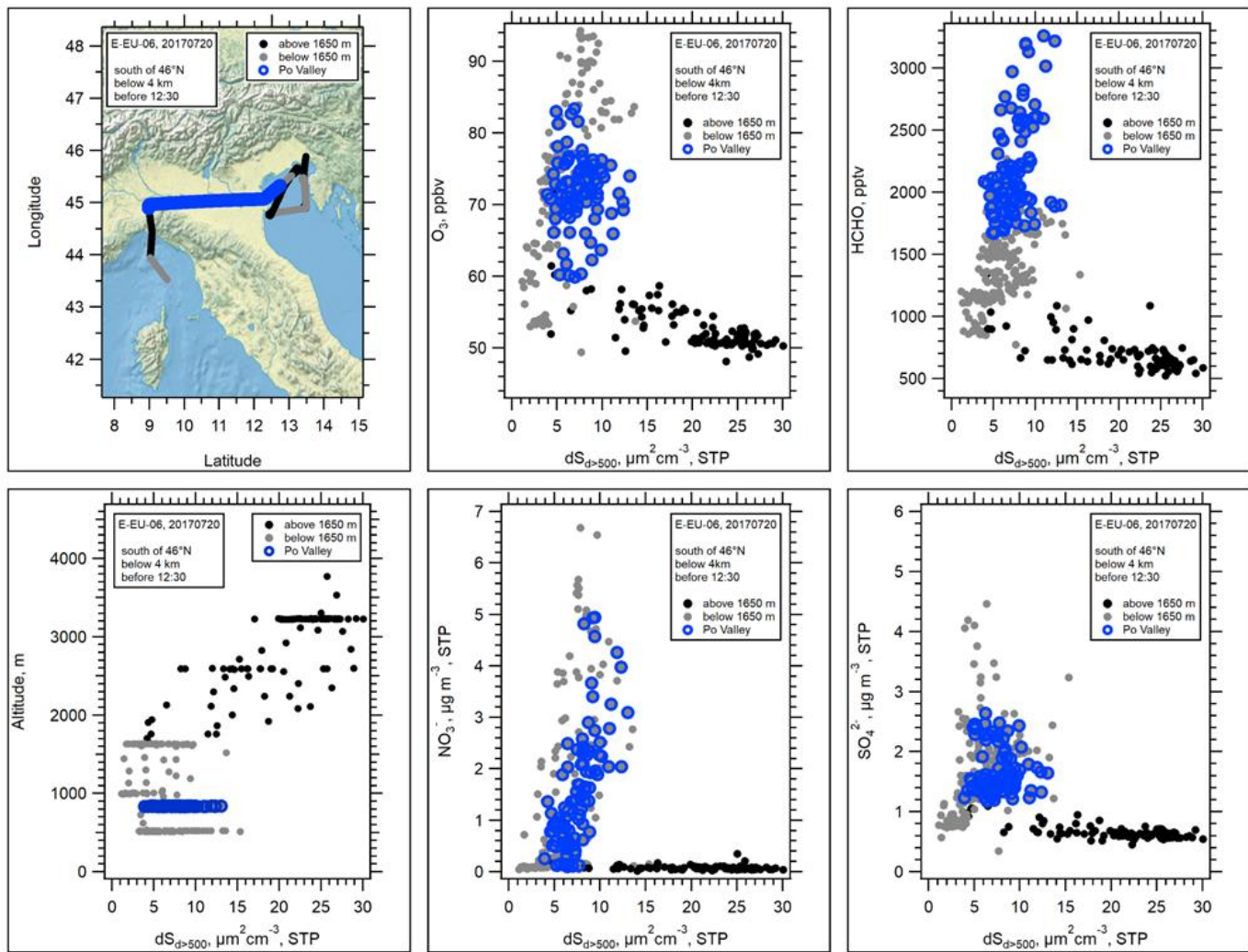
Correlations between the amount of selected species and  $dS_{d>500\text{nm}}$  were further investigated in an attempt to find some 685 indications of the effect of dust in heterogeneous processes. For this, HALO data across the Po Plain at 830-840 m altitude were selected when additional vertical information near the CPP was available. Figure 17 illustrates the measurement location and altitude as well as the vertical profile of  $dS_{d>500\text{nm}}$  (left column). The vertical profile shows that the main dust layer was above about 1650 m, in agreement with ALC data (Figure 14) and the BL height of about 1600 m (Table 1), but HALO encountered air masses with significant amounts of particles with  $d > 500$  nm also below that height. The plots in the upper 690 row of Fig. 17 show the gas-phase substances  $\text{O}_3$  and  $\text{HCHO}$  which both undergo heterogeneous reactions on dust (e.g., Wang et al., 2017) and should therefore decrease with increasing dust load. This behaviour is indeed observed above 1650 m (black dots), but not in the BL below 1600 m, where both species show a slightly positive correlation with  $dS_{d>500\text{nm}}$ . This may indicate that the BL source of both the particles with  $d > 500$  nm and the two gas-phase species was local pollution from the Po Plain, while above the boundary layer, heterogeneous removal of  $\text{O}_3$  and  $\text{HCHO}$  occurred.

695 In contrast,  $\text{NO}_3^-$  and  $\text{SO}_4^{2-}$  (lower row) show a positive correlation with  $dS_{d>500\text{nm}}$  in the BL over the Po Plain and the surrounding regions. Above the BL, where the particle surface area increased due to an increasing amount of dust particles (see LiDAR and ALC profiles in Fig. 14), both particulate species show no correlation with  $dS_{d>500\text{nm}}$  but remain constant at low concentration. Also, the mixing ratio of  $\text{SO}_2$ , which is the precursor gas for sulphate production, does not show a negative



correlation with  $dS_{d>500\text{nm}}$  above 1650 m (not shown). Whether the positive correlations in the BL are due to heterogeneous production or to common local sources cannot be answered from the current data set.

700 For all four species shown in Figure 17, the slope of the correlation with  $dS_{d>500\text{nm}}$  changes clearly between the BL and the FT. These observations are of interest for the validation of surface loss processes on aerosol models.



705 **Figure 17: Relation between mixing ratios or mass concentrations of selected species ( $O_3$ , HCHO,  $NO_3^-$ ,  $SO_4^{2-}$ ) and the surface area concentration of particles with diameter larger than 500 nm ( $dS_{d>500\text{nm}}$ ) measured during E-EU-06 on July 20, 2017. On the left side, the flight location and the observed vertical distribution of particles are shown. Dots for flight altitudes below and above 1650 m are shown in grey and black respectively while the blue colour indicates the CPP crossing at 830-840 m. Public domain GIS data available in Wavemetrics IgorPro.**



## 710 4 Summary and conclusions

Understanding the transport and transformation of pollutants is crucial for an adequate assessment of air quality and for the development of effective mitigation strategies for urban agglomerations. This is particularly important in the BL of highly polluted environments with complex topography.

715 The objective of this investigation was to undertake a case and investigate and characterise key primary and secondary pollutants in the Po Valley, which is a large urban agglomeration, an effective megacity, and both an industrial and agricultural centre. The study exploits the airborne observations of selected trace gases and particulate matter components during two EMeRGe flights carried out in the Po Plain from the Gulf of Venice to the Gulf of Genoa and the ground-based data from air quality and LiDAR networks in July 2017. The differences in mixing ratios and variability of the targeted species as well as the processing during the aging of the observed pollution plumes, as estimated by HYSPLIT dispersion simulations, provide 720 valuable information about the degree of mixing of the emissions within the BL and their photochemical transformation during transport.

725 The observations of major air pollutants and short-lived climate forcer precursors such as NO, NO<sub>2</sub>, CO and SO<sub>2</sub> at ground level indicated that the south of Lombardy and the surroundings of Milan are the most polluted areas in the central section of the Po Plain, CPP, which has a predominance of urban and traffic emission sources. The coastal areas of Genoa and Venice have in comparison significant emissions from shipping, as well as tourism and industrial activities near their ports.

Overall, stagnant conditions dominated in the CPP at the time of the investigated flights and advection of pollutants from the coastal areas into the CPP was favoured. Backward-trajectories indicated inland transport of emissions from the port of Genoa in agreement with the ground-based observations of pollutants and the SO<sub>2</sub>, CO and NO<sub>y</sub> plumes probed during the flights. In contrast, an apparent accumulation of local emissions was observed in the lower BL in the eastern part of the CPP, close to the 730 Gulf of Venice. The stagnant conditions resulted in a decoupling between the lower and the upper part of the BL causing concentration gradients. Thus, the content of reactive primary pollutants such as NO, NO<sub>2</sub> and SO<sub>2</sub> in the air masses probed onboard HALO in the upper BL was above the levels measured at ground-based background stations but lower than elsewhere along the flight tracks. These gradients are interpreted as examples of the transformation of the primary pollutants having a lower time constant than that of the vertical mixing within the BL, which is generally estimated to be about 20 to 30 minutes.

735 The distribution of secondary products and long-lived species such as O<sub>3</sub> and CO provide additional information about the transport and transformation of the probed air masses. The O<sub>3</sub> enhancements relative to the background in the lower and upper parts of the BL indicate that the photochemical processing of the emissions in the polluted plumes during the horizontal transport towards the Alps is similar to that during convective mixing in the BL of the Po Plain. Then again, vertical and horizontal gradients of long-lived species depend on the efficiency of the mixing within the BL.

740 Furthermore, the combined effect of Alpine venting and thermally driven advection to the coast resulted in a returning layer of pollution in the upper BL at 1600 m approximately. This layer was identified by residual plumes of long-lived trace gases and O<sub>3</sub> during the measurement period. These aged air masses are expected to be transported eastward by the synoptic-scale



circulation over the Po Plain above 2000 m and to affect air quality in Eastern Europe if they are fumigated back inside the BL.

745 The results show that HYSPLIT dispersion simulations using CO as a tracer provide a consistent picture with the regional transport and the degree of ageing of the observed pollution plumes but, importantly, are not able to simulate return layers close to the upper BL.

In this context of transboundary transport above the BL, the free troposphere over the Po Plain was additionally affected by a significant transport of dust from the Saharan desert. The present results indicate that mixing of dust layers with urban pollution 750 leads to changes in the losses of trace species on the particle surface and therefore affects the chemical transformation in the pollution plumes. Although direct evidence of heterogeneous production of nitrate and sulphate on the dust surface in the dust layer above the BL was not observed, the observations suggest desert dust transport could have played a role in weakening BL mixing and photochemistry (decreasing photolysis frequency values) and in trapping reactive species (e.g. O<sub>3</sub>).

Overall, the results obtained show the complexity of the transformation and transport of emissions from the Po Plain into the 755 BL and FT, which affects the primary and secondary air pollution. The study reinforces the necessity and relevance of airborne measurements of trace gases and aerosol constituents at different altitudes in combination with multiple radio soundings to complement the observations at the ground in the assessment of the amount of pollution and its effects on health, ecosystem services and agriculture. In addition, this study shows how local circulation patterns strongly influence these processes in the Po Valley in summer. While atmospheric chemistry models have improved greatly, continued model development and 760 experimental studies are still needed to better understand and predict pollution behaviour in complex terrain.

### Code, data, or code and data availability

The EMeRGe data are available at the HALO database (<https://doi.org/10.17616/R39Q0T> last accessed: 2025-12-22) and can be accessed upon registration. Further data can be made available upon request to the corresponding author.

### Supplement link

765 The supplement is provided as a separate document. The link to the supplement will be included by Copernicus.

### Author contributions

CC prepared the manuscript with contributions from all co-authors, MDAH, JPP, FB and JPB supervised the findings of this study and contributed significantly to manuscript revisions. HD provided COSMO-LAGRANTO and RB the HYSPLIT CO-enhancement calculations. JS, HZ, KK, JS, OOK, BH, BW, EF, MG, YL, DS, JW, AB, BB, KP provided data used in the



770 study. All authors have contributed to the manuscript, corrections, post-writing formatting, and revisions in reviewing and interpreting the results presented.

### Competing interests

At least one of the (co-)authors is a member of the editorial board of Atmospheric Chemistry and Physics.

775 The peer-review process was guided by an independent editor, and the authors also have no other competing interests to declare.

### Disclaimer

Copernicus Publications remains neutral with regard to jurisdictional claims made in the text, published maps, institutional affiliations, or any other geographical representation in this paper. While Copernicus Publications makes every effort to include appropriate place names, the final responsibility lies with the authors. Views expressed in the text are those of the authors and 780 do not necessarily reflect the views of the publisher.

### Special issue statement.

This article is intended to be part of the special issue “Effect of Megacities on the Transport and Transformation of Pollutants at Regional and Global Scales (EMeRGe) (ACP/AMT interjournal SI)”. It is not associated with a conference

### Acknowledgements

785 The authors thank all the teams and individuals without whom the EMeRGe campaign in Europe would not have been possible, especially the HALO flight coordination and BAHAMAS teams, and flight engineers. The contribution of local ARPA agencies by providing ground-based data from the Italian air quality network is gratefully acknowledged. Special thanks to Alessia Sannino and Antonella Boselli for providing the lidar data from Naples and San Pietro Capofiume and Angela Marioni for the data of the GLWF flight on 20.07.2017.

790 Luca Di Liberto (CNR-ISAC) and Luca Ferrero (University of Milan-Bicocca) are acknowledged for their support in the collection of ALICENET data in Milan.

Francesca Barnaba would like to thank the National Civil Aviation Agency (ENAC) for the support received in the authorization process of HALO flights over the Italian territory.

Dust images in Figure S13 were provided by the WMO Barcelona Dust Regional Center and the partners of the Sand and Dust 795 Storm Warning Advisory and Assessment System (SDS-WAS) for Northern Africa, the Middle East and Europe.



The authors gratefully acknowledge the NOAA Air Resources Laboratory (ARL) for the provision of the HYSPLIT transport and dispersion model and/or READY website (<https://www.ready.noaa.gov>) used in this publication. They also gratefully acknowledge the Institute for Atmospheric and Climate Science, ETH Zurich, Switzerland, for the provision of the LAGRANTO software

## 800 Financial support

This project was in part funded by the State and University of Bremen, the DLR Institute of Physics of the Atmosphere and the EMeRGe Project, which was part of the German Research Foundation DFG Priority Program (Schwerpunktprogramm) SPP 1294 "Atmospheric and Earth System Research with HALO" – "High Altitude and Long Range Research Aircraft". The funding of the HALO aircraft and the contributions to the various missions via DFG, the Max Planck Society (MPG), the 805 Helmholtz-Gemeinschaft, and the Deutsches Zentrum für Luft- und Raumfahrt (DLR; all from Germany) are highly acknowledged.

The scientific work of Klaus Pfeilsticker and Benjamin Weyland was supported by the DFG grants. PF-384/7-1, PF384/9-1, PF-384/16-1, PF-384/17, and PF-384/19. The scientific work of Katharina Kaiser and Johannes Schneider was supported by the DFG grants SCHN 1138/5-1 and BO 1829/10-1. The University of Bremen supported in part the EMeRGe measurements 810 and the contributions made by Midhun George, Yangzhuoran Liu, M. Dolores Andrés Hernández, and John Phillip Burrows. The article processing charges for this open-access publication were covered by the University of Bremen

## References

Agenzia regionale per la prevenzione, l'ambiente e l'energia dell'Emilia Romagna, Centro tematico regionale Qualità dell'aria. AGGIORNAMENTO DELL'INVENTARIO REGIONALE DELLE EMISSIONI IN ATMOSFERA DELL'EMILIA-815 ROMAGNA RELATIVO ALL'ANNO 2017 (INEMAR-ER 2017).Rapporto finale settembre 2020, 2020.

Andrés Hernández, M.D., Hilboll, A., Ziereis, H., Förster, E., Krüger, O.O., Kaiser, K., Schneider, J., Barnaba, F., Vrekoussis, M., Schmidt, J. and Huntrieser, H. Overview: On the transport and transformation of pollutants in the outflow of major population centres—observational data from the EMeRGe European intensive operational period in summer 2017. *Atmospheric Chemistry and Physics*, 22(9), pp.5877-5924, 2022.

820 APICE project, Report - Air Quality Status in Barcelona, Marseille, Genoa, Venice and Thessaloniki, (WP 3.2) TOTAL REPORT (<http://www.apice-project.eu/>), 2009.

ARPA Lombardia – Agenzia regionale per la Protezione dell'Ambiente, Settore Monitoraggi Ambientali, Centro Regionale Monitoraggio Qualità dell'Aria. Rapporto sulla qualità dell'aria della Città Metropolitana di Milano, Anno 2017.



ARPA Veneto – Dipartimento Regionale Qualità dell’Ambiente, Unità Organizzativa Qualità dell’Aria, Regione del Veneto  
825 – Area Tutela e Sicurezza del Territorio, Direzione Ambiente, UO Tutela dell’Atmosfera. Inventario Regionale delle Emissioni in Atmosfera in Regione Veneto, edizione 2017.

Ambrosetti, P., Anfossi, D., Cieslik, S., Graziani, G., Lamprecht, R., Marzorati, A., Nodop, K., Sandroni, S., Stingle, A., and Zimmermann, H.: Mesoscale transport of atmospheric trace constituents across the central Alps: TRANSALP tracer experiments. *Atmos. Environ.* 32 (7), 1257–1272, doi: 10.1016/S1352-2310(97)00185-4. 1998.

830 Athanasopoulou, E., Protonotariou, A. Papangelis, G. Tombrou, M. Mihalopoulos, N. Gerasopoulos, E: Long-range transport of Saharan dust and chemical transformations over the Eastern Mediterranean, *Atmospheric Environment*, Vol 140, 592-604, <https://doi.org/10.1016/j.atmosenv.2016.06.041>, 2016.

Baklanov A. MEGAPOLI Final Report, Part 1. 2011. Available at:[http://megapoli.dmi.dk/publ/MEGAPOLI\\_FinalReport\\_Part1.pdf](http://megapoli.dmi.dk/publ/MEGAPOLI_FinalReport_Part1.pdf).

835 Baklanov A., and Mahura A. Eds., MEGAPOLI Project Scientific Report 10-10: Interactions between Air Quality and Meteorology, MEGAPOLI Deliverable D4.3. Available at: [http://megapoli.dmi.dk/publ/MEGAPOLI\\_sr10-10.pdf](http://megapoli.dmi.dk/publ/MEGAPOLI_sr10-10.pdf), 2010.

Barnaba, F., and G. P. Gobbi, Aerosol seasonal variability over the Mediterranean region and relative contribution of maritime, continental and Saharan dust particles over the basin from MODIS data in the year 2001, *Atmospheric Chemistry and Physics*, 4, 2367-2391, 2004.

840 Barnaba, F., Gobbi, G.P. , de Leeuw, G., Aerosol stratification, optical properties and radiative forcing in Venice (Italy) during ADRIEX. *Q.J.R. Meteorol. Soc.*, 133: 47-60. <https://doi.org/10.1002/qj.91>, 2007.

Barnaba, F., Putaud, J. P., Gruening, C., dell’Acqua, A., and Dos Santos, S.: Annual cycle in co-located in situ, total-column, and height resolved aerosol observations in the Po Valley (Italy): Implications for ground-level particulate matter mass concentration estimation from remote sensing. *J. Geophys. Res.*, 115, doi: 10.1029/2009JD013002, 2010.

845 Barnaba, F., Romero, N.A., Bolignano, A., Basart, S., Renzi, M. and Stafoggia, M.: Multiannual assessment of the desert dust impact on air quality in Italy combining PM10 data with physics-based and geostatistical models. *Environment International*, 163, 107204, 2022.

Bellini, A., Diémoz, H., Di Liberto, L., Gobbi, G. P., Bracci, A., Pasqualini, F., and Barnaba, F.: ALICENET – an Italian network of automated lidar ceilometers for four-dimensional aerosol monitoring: infrastructure, data processing, and  
850 applications, *Atmos. Meas. Tech.*, 17, 6119–6144, <https://doi.org/10.5194/amt-17-6119-2024>, 2024.

Birmili, W., Heinke, K., Pitz, M., Matschullat, J., Wiedensohler, A., Cyrys, J., Wichmann, H.E. and Peters, A.: Particle number size distributions in urban air before and after volatilisation. *Atmospheric Chemistry and Physics*, 10, 4643-4660, 2010.

Butler, T. M., Lawrence, M. G., Gurjar, B., Aardenne, J. v., Schultz, M., and Lelieveld, J.: The representation of emissions from megacities in global emissions inventories. *Atmospheric Environment*, 42, 703-719, doi: 10.1016/j.atmosenv.2007  
855 .09.060, 2008.

Butler, T.M., and Lawrence, M.G.: The influence of megacities on global atmospheric chemistry: a modelling study. *Environ. Chem.* 6, 219e225, doi: 10.1071/EN09110. 2009.



Butler, T. M., Stock, Z. S., Russo, M. R., Denier van der Gon, H. A. C., and Lawrence, M. G. : Megacity ozone air quality under four alternative future scenarios. *Atmos. Chem. Phys.*, 12, 4413–4428, doi: 10.5194/acp-12-4413-2012, 2012.

860 Castaldini, D., Marchetti, M., Norini, G., Vandelli, V., and Zuluaga Vélez M. C.: Geomorphology of the central Po Plain, Northern Italy. *Journal of Maps*, 15:2, 780-787, doi: 10.1080/17445647.2019.1673222, 2019.

CityZen, 2011. megaCITY e Zoom for the ENvironment, THEME FP7-ENV2007.1.1.2.1: Megacities and Regional Hot-spots Air Quality and Climate. <http://cityzen-project.eu/>, 2011.

865 Collaud Coen, M., Praz, C., Haefele, A., Ruffieux, D., Kaufmann, P. and Calpini, B. : Determination and climatology of the planetary boundary layer height above the Swiss plateau by in situ and remote sensing measurements as well as by the COSMO-2 model, *Atmos. Chem. and Phys.*, 14(23), 13205-13221, 2014.

Contini, D., Gambaro, A., Belosi, F., De Pieri, S., Cairns, W.R.L., Donateo, A., Zanotto, E. and Citron, M.: The direct influence of ship traffic on atmospheric PM2. 5, PM10 and PAH in Venice. *Journal of Environmental Management*, 92(9), 2119-2129, 2011.

870 Curci, G., Ferrero, L., Tuccella, P., Barnaba, F., Angelini, F., Bolzacchini, E., Carbone, C., Denier van Der Gon, H.A.C., Facchini, M.C., Gobbi, G.P. , Kuenen, J.P.P. et al. : How much is particulate matter near the ground influenced by upper-level processes within and above the PBL? A summertime case study in Milan (Italy) evidences the distinctive role of nitrate. *Atmospheric Chemistry and Physics*, 15(5), pp.2629-2649, 2015.

DeMott, P.J., Prenni, A.J., Liu, X., Kreidenweis, S.M., Petters, M.D., Twohy, C.H., Richardson, M.S., Eidhammer, T., and 875 Rogers, D.C.: Predicting global atmospheric ice nuclei distributions and their impacts on climate, *Proc. Nat. Academy of Sci.*, PNAS, 107, 25, 11217–11222, 2010.

De Wekker, S.F. and Kossmann, M.: Convective boundary layer heights over mountainous terrain—a review of concepts. *Frontiers in Earth Science*, 3, p.77, 2015.

880 De Wekker, S.F.J., Kossmann, M., Knievel, J.C., Giovannini, L., Gutmann, E.D., Zardi, D.: Meteorological Applications Benefiting from an Improved Understanding of Atmospheric Exchange Processes over Mountains, *Atmosphere*, 9, 371, <https://doi.org/10.3390/atmos9100371>, 2018.

Diémoz, H., Barnaba, F., Magri, T., Pession, G., Dionisi, D., Pittavino, S., Tombolato, I. K. F., Campanelli, M., Della Ceca, L. S., Hervo, M., Di Liberto, L., Ferrero, L., and Gobbi, G. P.: Transport of Po Valley aerosol pollution to the north-western Alps – Part 1: Phenomenology. *Atmos. Chem. Phys.*, 19, 3065–3095, doi: 10.5194/acp-19-3065-2019, 2019a.

885 Diémoz, H., Gobbi, G. P, Magri, T., Pession, G., Pittavino, S., Tombolato, I. K. F., Campanelli, and. Barnaba, F: Transport of Po Valley aerosol pollution to the north-western Alps – Part 2: Long-term impact on air quality. *Atmos. Chem. Phys.*, 19, 10129–10160, doi: 10.5194/acp-19-10160-2019, 2019b.

Ferrero, L., Riccio, A., Ferrini, B.S., D'Angelo, L., Rovelli, G., Casati, M., Angelini, F., Barnaba, F., Gobbi, G.P., Cataldi, M. and Bolzacchini, E.: Satellite AOD conversion into ground PM10, PM2. 5 and PM1 over the Po valley (Milan, Italy) exploiting 890 information on aerosol vertical profiles, chemistry, hygroscopicity and meteorology. *Atmospheric Pollution Research*, 10(6), 1895-1912, 2019.



Finardi, S., and Pellegrini, U.: Systematic analysis of meteorological conditions causing severe urban air pollution episodes in the central Po Valley. In Proceedings of the 9th Int. Conf. on Harmonisation within Atmospheric Dispersion Modelling for Regulatory Purposes, Garmish-Partenkirchen, Germany, June 2004; pp. 250–254. Available at <http://www.harmo.org/conference.php?id=9>. 2004.

Finardi, S., Silibello, C., D'Allura, A., and Radice, P.: Analysis of pollutants exchange between the Po Valley and the surrounding European region. *Urban Clim.*, 10, 682 – 702, doi: 10.1016/j.uclim.2014.02.002, 2014.

Finardi, S., Agrillo, G., Baraldi, R., Calori, G., Carlucci, P., Ciccioli, P., D'Allura, A., Gasbarra, D., Gioli, B., Magliulo, V., Radice, P., Toscano, P., and Zaldei, A.: Atmospheric dynamics and ozone cycle during sea breeze in a Mediterranean complex urbanized coastal site. *Journal of Applied Meteorology and Climatology*, 57(5), 1083–1099, doi: 10.1175/JAMC-D-17-0117.1, 2018.

Folberth, G.A., Rumbold, S.T., Collins, W.J., and Butler, T.M. : Global radiative forcing and megacities. *Urban Clim.* 1, 4e19, doi: 10.1016/j.uclim.2012.08.001, 2012.

Georgiadis, T., Giovanelli, G., and Fortezza, F., Vertical layering of photochemical ozone during land-sea breeze transport. II *Nuovo Cimento C*, 17, 371-375, doi: 10.1007/BF02509176, 1994.

Gobbi, G. P., Barnaba, F., Van Dingenen, R., Putaud, J. P., Mircea, M., and Facchini, M. C.: Lidar and in situ observations of continental and Saharan aerosol: closure analysis of particles optical and physical properties, *Atmos. Chem. Phys.*, 3, 2161–2172, <https://doi.org/10.5194/acp-3-2161-2003>, 2003.

Gobbi, G.P., Di Liberto, L., Barnaba, F.: Impact of port emissions on EU-regulated and non-regulated air quality indicators: The case of Civitavecchia (Italy), *Science of the Total Environment*, 719, <https://doi.org/10.1016/j.scitotenv.2019.134984>, 2020.

Gohm, A., Harnisch, F., Vergeiner, J., Obleitner, F., Schnitzhofer, R., Hansel, A., Fix, A., Neininger, B., Emeis, S., and Schäfer, K.: Air Pollution Transport in an Alpine Valley: Results From Airborne and Ground-Based Observations, *Bound.-Lay. Meteorol.*, 131, 441–463, doi: 10.1007/s10546-009-9371-9, 2009.

Gonzalez Ortiz, A., Guerreiro, C. and Soares, J., Air Quality in Europe – EEA: 2020 Report, Tech. rep.N09/2020. doi: 10.2800/786656, 2020

Guimbaud, C., Arens, F., Gutzwiller, L., Gaggeler, H. W. and Ammann, M.: Uptake of  $\text{HNO}_3$  to deliquescent sea-salt particles: a study using the short-lived radioactive isotope tracer  $^{13}\text{N}$ , *Atmos. Chem. Phys.*, 2, 249–257, 2002.

Gurjar, B.R., and Lelieveld, J.: New directions: megacities and global change. *Atmos. Environ.* 39, 391–393. doi: 10.1016/j.atmosenv.2004.11.002, 2005.

Helbig, M., Gerken, T, Beamesderfer. E.R., Baldocchi, D.D., Banerjee, T., Biraud, S.C., Brown, W.O.J., Brunsell, N.A., Burakowski, E.A., Burns, S.P., Butterworth, B.J., Chan, S., Davis, K.J., Desai, A.R., Fuentes, J.D., Hollinger, D.Y., Kljun, N., Mauder, M., Novick, K.A., Perkins, J.M., Rahn, D.A., Sanchez, C-R., Santanello, J.A., Scott, R.L., Seyednasrollah, B., Stoy., P.C., Sullivan, R.C., Vilà-Guerau de Arellano, J., Wharton, S., Yi, C., Richardson, A.D.: Integrating continuous atmospheric



925 boundary layer and tower-based flux measurements to advance understanding of land-atmosphere interactions, Agricultural and forest Meteorology, 307, <https://doi.org/10.1016/j.agrformet.2021.108509>, 2021.

Henne, S., Furger, M., Nyeki, S., Steinbacher, M., Neininger, B., de Wekker, S. F. J., Dommen, J., Spichtinger, N., Stohl, A., and Prévôt, A. S. H.: Quantification of topographic venting of boundary layer air to the free troposphere, *Atmos. Chem. Phys.*, 4, 497–509, doi: 10.5194/acp-4-497-2004, 2004.

930 Henne, S., Dommen, J., Neininger, B., Reimann, S., Staehelin, J., and Prévôt, A. S. H.: Influence of mountain venting in the Alps on the ozone chemistry of the lower free troposphere and the European pollution export, *Journal of Geophys. Res.*, Vol 110, D22307 doi: 10.1029/2005JD005936, 2005.

Hennemuth, B., and Lammert-Stockschlaeder, A.: Determination of the Atmospheric Boundary Layer Height from Radiosonde and Lidar Backscatter. *Boundary-Layer Meteorology*, v.120, 181-200, doi: 120. 10.1007/s10546-005-9035-3, 2006.

935 Hersbach, H., Bell, B., Berrisford, P., Hirahara, S., Horányi, A. Muñoz- Sabater, J. et al., The ERA5 global reanalysis, *Quart. J. Royal Meteoro. Soc.*, 2020, <https://doi.org/10.1002/qj.3803>

Highwood, E.J., Haywood, J.M., Coe, H., Cook, J., Osborne, S., Williams, P., Crosier, J., Bower, K., Formenti, P., McQuaid, J., Brooks, B., Thomas, G., Grainger, R., Barnaba, F., Gobbi, GP., De Leeuw, G: Aerosol direct radiative impact experiment (ADRIEX) overview. *Quarterly Journal of the Royal Meteorological Society*, 133(S1), 3-15, 2007.

940 Hong, Q., Liu, C., Hu, Q., Zhang, Y., Xing, C. , Su, W., Ji, X., Xiao, S.: Evaluating the feasibility of formaldehyde derived from hyperspectral remote sensing as a proxy for volatile organic compounds *Atmospheric Research*, 264, <https://doi.org/10.1016/j.atmosres.2021.105777>, 2021.

Hüneke, T., Aderhold, O.-A., Bounin, J., Dorf, M., Gentry, E., Grossmann, K., Grooß, J.-U., Hoor, P., Jöckel, P., Kenntner, M., Knapp, M., Knecht, M., Lörks, D., Ludmann, S., Matthes, S., Raecke, R., Reichert, M., Weimar, J., Werner, B., Zahn, A.,

945 Ziereis, H., and Pfeilsticker, K.: The novel HALO mini-DOAS instrument: inferring trace gas concentrations from airborne UV/visible limb spectroscopy under all skies using the scaling method, *Atmos. Meas. Tech.*, 10, 4209–4234, 80 <https://doi.org/10.5194/amt-10-4209-2017>, 2017.

ISTAT, *Annuario statistico Italiano* 2022.

Itahashi, S., Hattori, S., Ito, A., Sadanaga, Y., Yoshida, N., and Matsuki, A.: Role of Dust and Iron Solubility in Sulfate Formation during the Long-Range Transport in East Asia Evidenced by  $^{17}\text{O}$ -Excess Signatures, *Environ. Sci. Technol.* 2022, 56, 13634-13643, <https://doi.org/10.1021/acs.est.2c03574>, 2022.

Karydis, V.A., Tsimpidi, A.P., Pozzer, A., Astitha, M., and Lelieveld, J.: Effects of mineral dust on global atmospheric nitrate concentrations, *Atmos. Chem. Phys.*, 16, 1491-1509, doi:10.5194/acp-16-1491-2016, 2016.

Kluge, F., Hüneke, T., Knecht, M., Lichtenstern, M., Rotermund, M., Schlager, H., Schreiner, B., and Pfeilsticker, K.: Profiling 955 of formaldehyde, glyoxal, methylglyoxal, and CO over the Amazon: normalized excess mixing ratios and related emission factors in biomass burning plumes, *Atmos. Chem. Phys.*, 20, 12363–12389, <https://doi.org/10.5194/acp-20-12363-2020>, 2020.

Lawrence, M.G., Butler, T.M., Steinkamp, J., Gurjar, B.R., and Lelieveld, J.: Regional pollution potentials of megacities and other major population centres. *Atmos. Chem. Phys.* 7, 3969e3987, doi: 10.5194/acp-7-3969-2007, 2007.



Maclean, A.M. Butenhoff, C.L., Grayson, J.W., Barsanti, K., Jimenez, J.L. and Bertram, A.K.: mixing times of organic  
960 molecules within secondary organic aerosol particles: a global planetary boundary layer perspective, *Atmos. Chem. Phys.* 17,  
13037-13048, 2017. <https://doi.org/10.5194/acp-17-13037-2017>.

Marenco, F., Bonasoni, P., Calzolari, F., Ceriani, M., Chiari, M., Cristofanelli, P., D'Alessandro, A., Fermo, P., Lucarelli, F.,  
Mazzei, F. and Nava, S.: Characterization of atmospheric aerosols at Monte Cimone, Italy, during summer 2004: source  
apportionment and transport mechanisms. *Journal of Geophysical Research: Atmospheres*, 111(D24), 2006.

965 Marmer, E. and Langmann, B.: Impact of ship emissions on the Mediterranean summertime pollution and climate: A regional  
model study. *Atmospheric Environment*, 39(26), 4659-4669, 2005.

McKendry, I.G. and Lundgren, J.: Tropospheric layering of ozone in regions of urbanized complex and/or coastal terrain: a  
review. *Progress in Physical Geography*, 24(3), pp.329-354. 2000.

MEGAPOLI. Megacities: Emissions, Urban, Regional and Global Atmospheric POLLution and Climate Effects, and Integrated  
970 Tools for Assessment and Mitigation, THEME FP7-ENV-2007.1.1.2.1: Megacities and Regional Hot-spots Air Quality and  
Climate. <http://megapoli.dmi.dk/>.2011.

Merico E., Conte M., Grasso F.M., Cesari D., Gambaro A., Morabito E., Gregoris E., Contini D.: Trends of Shipping Impact  
to Particulate Matter in Two Adriatic Port-Cities. *Environmental Sciences Proceedings*; 8(1):10. <https://doi.org/10.3390/ecas2021-10343>, 2021.

975 Millán, M.M., Salvador, R., Mantilla, E., and Kallos, G.: Photooxidant dynamics in the Mediterranean basin in summer:  
Results from European research projects. *Journal of Geophysical Research*, 102, 8811-8823, doi: 10.1029/96JD03610. 1997.

Millán, M. M., Mantilla, E., Salvador, R., Carratalá, A., Sanz, M. J., Alonso, L., Gangoiti, G., and Navazo, M. ; Ozone Cycles  
in the Western Mediterranean Basin: Interpretation of Monitoring Data in Complex Coastal Terrain, *Journal of Applied  
Meteorology*, 39(4), 487-508, doi: 10.1175/1520-0450(2000)0392.0.CO;2, 2000.

980 Millán, M. M, Sanz, M. J., Salvador, R., and Mantilla, E.: Atmospheric dynamics and ozone cycles related to nitrogen  
deposition in the western Mediterranean. *Environ Pollut.*, 118(2):167-86. doi: 10.1016/s0269-7491(01)00311-6. PMID:  
11939281, 2002.

Molina M. J. and Molina L. T.: Megacities and Atmospheric Pollution. *Journal of the Air and Waste Management Association*,  
54:6, 644-680, doi: 10.1080/10473289.2004.10470936. 2004.

985 Nyeki, S., Eleftheriadis, K., Baltensperger, U., Colbeck, I., Fiebig, M., Fix, A., Kiemle, C., Lazaridis, M., and Petzold, A.:  
Airborne Lidar and in-situ Aerosol Observations of an Elevated Layer, Leeward of the European Alps and Apennines,  
*Geophys. Res. Lett.*, 29, 33-1–33-4, doi: 10.1029/2002GL014897. 2002.

Pederzoli, A., Mircea, M., Finardi, S., di Sarra, A., Zanini, G.; Quantification of Saharan dust contribution to PM10  
concentrations over Italy during 2003-2005, *Atmospheric Environment*, 44, 4181-4190, <https://doi.org/10.1016/j.atmosenv.2010.07.031> 2010.

990 Putaud, J. P., Cavalli, F., Martins dos Santos, S., and Dell'Acqua, A.: Long-term trends in aerosol optical characteristics in the  
Po Valley, Italy, *Atmos. Chem. Phys.*, 14, 9129–9136, doi: 10.5194/acp-14-9129-2014. 2014.



Raffaelli, K., Deserti, M., Stortini, M., Amorati, R., Vasconi, M., and Giovannini, G.: Improving Air Quality in the Po Valley, Italy: Some Results by the LIFE-IP-PREPAIR Project. *Atmosphere*, 11, 429, doi: 10.3390/atmos11040429, 2020.

995 Rotach, M. W., and Coauthors: Turbulence Structure and Exchange Processes in an Alpine Valley: The Riviera Project. *Bull. Amer. Meteor. Soc.*, 85, 1367–1386, <https://doi.org/10.1175/BAMS-85-9-1367>, 2004.

Schroeder, J.R., Crawford, J.H., Fried, A., Walega, J., Weinheimer, A., Wisthaler, A.: New insights into the column  $\text{CH}_2\text{O}/\text{NO}_2$  ratio as an indicator of near-surface ozone sensitivity. *J. Geophys. Res. Atmos.* 122, 8885–8907. <https://doi.org/10.1002/2017jd026781>, 2017.

1000 Seibert, P., Beyrich, F., Gryning, S-E., Joffre, S., Rasmussen, A., and Tercier, P.: Review and intercomparison of operational methods for the determination of the mixing height. *Atmospheric Environment*, 34(7), 1001-1027, doi: 10.1016/S1352-2310(99)00349-0, 2000.

Sillman, S.: The use of  $\text{NO}_y$ ,  $\text{H}_2\text{O}_2$ , and  $\text{HNO}_3$  as indicators for ozone- $\text{NO}_x$  hydrocarbon sensitivity in urban locations. *J. Geophys. Res. Atmos.* 100, 14175–14188. <https://doi.org/10.1029/94jd02953>, 1995.

1005 Simon, H., Valin, L.C., Baker, K.R., Henderson, B.H., Crawford, J.H., Pusede, S.E., Kelly, J.T., Foley, K.M., Chris Owen, R., Cohen, R.C. and Timin, B.: Characterizing CO and  $\text{NO}_y$  sources and relative ambient ratios in the Baltimore area using ambient measurements and source attribution modeling. *Journal of Geophysical Research: Atmospheres*, 123(6), 3304-3320, 2018.

Souri, A. H., Nowlan, C.R., Wolfe, G.M., Lamsal, L.N., Miller, C.E.C., Gonzalez Abad, G., Janz, S.J., Fried, A., Blake, D. R., Weinheimer, A. J., Diskin, G.S. Liu, X. Chance, K.: Revisiting the effectiveness of  $\text{HCHO}/\text{NO}_2$  ratios for inferring ozone sensitivity to its precursors using high resolution airborne remote sensing observations in a high ozone episode during the KORUS-AQ campaign. *Atmos. Environ.* 224, 117341, 2020.

Sprenger, M. and Wernli, H.: The LAGRANTO Lagrangian analysis tool—version 2.0. *Geoscientific Model Development*, 8(8), pp.2569-2586, 2015.

1015 Stohl, A., and Wotawa, G.: A method for computing single trajectories representing boundary layer transport. *Atmospheric Environment*, 29(22), 3235-3238, doi: 10.1016/1352-2310(95)00259-2. 1995.

Stohl, A., Wotawa, G., Seibert, P., and Kromp-Kolb, H.: Interpolation errors in wind fields as a function of spatial and temporal resolution and their impact on different types of kinematic trajectories. *Journal of Applied Meteorology and Climatology*, 34(10), 2149-2165, doi: 10.1175/1520-0450(1995)0342.0.CO;2, 1995.

1020 Stortini M., Deserti M., Bonafè G., and Minguzzi E.: Long-term simulation and validation of ozone and aerosol in the Po Valley. In: Borrego C, Renner E (Eds.) *Developments in environmental sciences*, vol. 6, pp 768-770. Elsevier, 2007.

Talbot, N., Kubelova, L., Makes, O., Cusack, M., Ondracek, J., Vodička, P., Schwarz, J., Zdimal, V.: Outdoor and indoor aerosol size, number, mass and compositional dynamics at an urban background site during warm season, *Atmos. Environ.*, 131m 171-184, <http://dx.doi.org/10.1016/j.atmosenv.2016.01.055>, 2016.

1025 Tampieri, F., Trombetti, F., and Scarani, C.: Summer daily circulation in the Po Valley, Italy, *Geophysical & Astrophysical Fluid Dynamics*, 17:1, 97-112, doi: 10.1080/03091928108243675.1981.



Targa, J., Colina, M., Banyuls, L., González Ortiz, A., Soares, J.: Status report of air quality in Europe for year 2023, using validated and up-to-date data (ETC-HE Report 2024/5). European Topic Centre on Human Health and the Environment, 2024.

Valin, L.C., Russell, A.R., and Cohen, R.C.: Variations of OH radical in an urban plume inferred from NO<sub>2</sub> column measurements, *Geophys. Res. Letters*, 40, 1856–1860, doi:10.1002/grl.50267, 2013.

1030 Van Dingenen, R., Putaud, J.P, Martins-Dos Santos, S., and Raes, F.: Physical aerosol properties and their relation to air mass origin at Monte Cimone (Italy) during the first MINATROC campaign, *Atmos. Chem. Phys.*, 5, <https://doi.org/10.5194/acp-5-2203-2005>, 2005.

Vazquez Santiago, J., Hata, H., Martinez-Noriega, E. and Inoue, K., Ozone trends and their sensitivity in global megacities under the warming climate, *nature communications*, <https://doi.org/10.1038/s41467-024-54490-w>, 2024.

1035 Wandinger, U.: Introduction to lidar. In *Lidar: range-resolved optical remote sensing of the atmosphere* (pp. 1-18). New York, NY: Springer New York, 2005.

Wang, X. Y., and Wang, K. C.: Estimation of atmospheric mixing layer height from radiosonde data, *Atmos. Meas. Tech.*, 7, 1701–1709, doi: 10.5194/amt-7-1701-2014, 2014.

Wang, Z., Pan, X., Uno, I., li, J., Wang, Z., Chen, X., Fu, P., Yang, T., Kobayashi, H., Shimizu, A., Sugimoto, N., Yamamoto, S., 1040 Significant impacts of heterogeneous reactions on the chemical composition and mixing state of dust particles: A case study during dust events over northern China, *Atmospheric Environment*, 159, 83-91, <https://doi.org/10.1016/j.atmosenv.2017.03.044>, 2017.

Wang, Y., Ma, Y.-F., Muñoz-Esparza, D., Li, C. W. Y., Barth, M., Wang, T., and Brasseur, G. P.: The impact of inhomogeneous emissions and topography on ozone photochemistry in the vicinity of Hong Kong Island, *Atmos. Chem. Phys.*, 21, 3531–3553, <https://doi.org/10.5194/acp-21-3531-2021>, 2021.

1045 Wang, Y., Brasseur, G.P. and Wang, T.: Segregation of atmospheric oxidants in turbulent urban environments. *Atmosphere* 13 (2), p.315, 2022.

Weger, M., Heinold, B., Engler, Ch., Schumann, U., Seifert, A., Fößig, R., Voigt, Ch., Baars, H., Blahak, U., Borrmann, S., Hoose, C., Kaufmann, S., Krämer, M., Seifert, P., Senf, F., Schneider, J., and Tegen, I.: The impact of mineral dust on cloud 1050 formation during the Saharan dust event in April 2014 over Europe, *Atmos. Chem. Phys.*, 18, 17545–17572, <https://doi.org/10.5194/acp-18-17545-2018>, 2018.

Weissmann, M., Braun, F. J., Gantner, L., Mayr, G. J., Rahm, S., and Reitebuch, O.: The Alpine Mountain–Plain Circulation: Airborne Doppler Lidar Measurements and Numerical Simulations, *Monthly Weather Review*, 133(11), 3095-3109. Retrieved from <https://journals.ametsoc.org/view/journals/mwre/133/11/mwr3012>. 2005.

1055 Wotawa, G., Kröger, H., and Stohl, A.: Transport of ozone towards the Alps – results from trajectory analyses and photochemical model studies, *Atmos. Environ.* , 34, 1367 – 1377, doi: 10.1016/S1352-2310(99)00363-5. 2000.

Yus-Díez, J., Ealo, M., Pandolfi, M., Perez, N., Titos, G., Močnik, G., Querol, X., and Alastuey, A. Aircraft vertical profiles during summertime regional and Saharan dust scenarios over the north-western Mediterranean basin: aerosol optical and physical properties, *Atmos. Chem. Phys.*, 21, 431–455, doi: 10.5194/acp-21-431-2021, 2021.



1060 Zhang, Y., Luo, G., & Yu, F.: Seasonal variations and long-term trend of dust particle number concentration over the northeastern United States. *Journal of Geophysical Research: Atmospheres*, 124, 13,140–13,155. <https://doi.org/10.1029/2019JD031388>, 2019.

Zhu, S., Butler, T., Sander, R., Ma, J., and Lawrence, M. G.: Impact of dust on tropospheric chemistry over polluted regions: a case study of the Beijing megacity, *Atmos. Chem. Phys.*, 10, 3855–3873, <https://doi.org/10.5194/acp-10-5121-2010>, 2010.